European Journal of Pharmaceutics and Biopharmaceutics 193 (2023) 241–253

Contents lists available at ScienceDirect

European Journal of Pharmaceutics and Biopharmaceutics

journal homepage: www.elsevier.com/locate/ejpb

Research paper

Improved antitumor activity through a tyramidyl maslinic acid derivative. Design and validation as drug-loaded electrospun polymeric nanofibers

Cristina Luque [a,b,c], María de la Cabeza Fernández [d], David Fuentes-Rios [e], Ana Cepero [a,b,c], Rafael Contreras-Cáceres [f,*], Manuel Doña [e], Gloria Perazzoli [a,b,c], Laura Lozano-Chamizo [d,g], Marco Filice [d], Marzia Marciello [d], Victor Gonzalez-Rumayor [g], Juan Manuel López-Romero [e], Laura Cabeza [a,b,c,*], Consolación Melguizo [a,b,c], José Prados [a,b,c]

[a] Institute of Biopathology and Regenerative Medicine (IBIMER), Center of Biomedical Research (CIBM), University of Granada, Granada 18100, Spain
[b] Department of Anatomy and Embryology, Faculty of Medicine, University of Granada, Granada 18071, Spain
[c] Biosanitary Institute of Granada (ibs. GRANADA), Granada 18014, Spain
[d] Nanobiotechnology for Life Sciences Laboratory, Department of Chemistry in Pharmaceutical Science, Faculty of Pharmacy, Universidad Complutense de Madrid (UCM), Plaza Ramón y Cajal s/n, E-28040 Madrid, Spain
[e] Department of Organic Chemistry, Faculty of Sciences, University of Malaga, 29071 Málaga, Spain
[f] Department of Chemistry and Physics, University of Almería, 04120, Spain
[g] Atrys Health, E-28001 Madrid, Spain

ARTICLE INFO

Keywords:
Electrospun polymer nanofibers
Localized drug release
Colorectal cancer
Breast cancer
Chemotherapy
Tyramine-maslinic acid

ABSTRACT

Among the most harmful tumors detected in the human body, such as breast, colon, brain or pancreas, breast (BC) and colorectal cancer (CRC) are the first and third most frequent cancer worldwide, respectively. The current existing chemotherapeutic treatments present serious side effects due to their intravenous administration can induce cytotoxicity in healthy cells. Thus, new treatment methods based on drug-loaded polymeric nanofibers (NFs) have gained significant potential for their use in localized cancer chemotherapy. Here, a deep in vitro comparative analysis between maslinic acid (MA) and a tyramine-maslinic acid (TMA) derivative is initially performed. This analysis includes a proliferation, and a cell cycle assay, and a genotoxicity, antiangiogenic and apoptosis study. Then, the TMA derivative has been incorporated into electrospun polymeric NFs obtaining an implantable dressing material with antitumor activity. Two types of patches containing TMA-loaded polymeric NFs of poly(caprolactone) (PCL), and a mixture of polylactic acid/poly(4-vinylpyridine) (PLA/PVP) were fabricated by the electrospinning technique. The characterization of the drug-loaded NFs showed an encapsulation capacity of 0.027 mg TMA/mg PCL and 0.024 mg TMA/mg PLA/PVP. Then, the cytotoxic activity of both polymeric systems was tested in CRC (T84), BC (MCF-7) and a no tumor (L929) cell lines exposed to TMA-loaded NFs and blank NFs for 48 h. Moreover, cell cycle assay, genotoxicity, angiogenesis and apoptosis tests were carried out to study the mechanism of action of TMA. Blank NFs showed no-toxicity in all cell lines tested and both drug-loaded NFs significantly reduced cell proliferation (relative proliferation of ≈44 % and ≈25 % respectively). Therefore, TMA was less genotoxic than maslinic acid (MA), and reduced VEGFA expression in MCF-7 cells (1.32 and 2.12-fold for MA and TMA respectively). These results showed that TMA-loaded NFs could constitute a promising biocompatible and biodegradable nanoplatform for the local treatment of solid tumors such as CRC or BC.

Abbreviations: PLA/PVP, Poly (lactic acid)/poly(4-vinylpyridine); BC, Breast; CAM, Chorioallantoic membrane; JNK, C-Jun NH2-terminal kinase; CRC, Colorectal cancer; DCM, Dichloromethane; DMF, Dimethylformamide; DOX, Doxorubicin; DMEM, Dulbecco's Modified Eagle's Medium; FBS, Fetal bovine serum; FDA, Food and Drug Administration; γH2AX, H2AX phosphorylation; IC50, Half-maximal inhibitory concentration; HPLC, High performance liquid chromatography; LDD, Localized drug delivery; MA, Maslinic acid; NFs, Nanofibers; OD, Optical density; PBS, Phosphate buffered saline solution; PAM, Polyacrylamide; PCL, Poly(caprolactone); PEG, Poly(ethylene glycol); PEO, Poly(ethylene oxide); PLA, Poly(lactic acid); PLGA, Poly(lactic-co-glycolic acid); PVA, Poly(vinyl alcohol); PVP, Poly (vinyl pyridine); SD, Standard deviation; SPSS, Statistical Package for the Social Sciences; SRB, Sulforhodamine B; TCA, Trichloroacetic acid; TBS, Tris-Buffered Saline; TMA, Tyramine-maslinic acid; TMA-NFs, Tyramine-maslinic acid-loaded nanofibers; VEGFA., Vascular endothelial growth factor A.

* Corresponding authors at: Institute of Biopathology and Regenerative Medicine (IBIMER), Center of Biomedical Research (CIBM), University of Granada. Department of Chemistry and Physics, University of Almería, 04120, Spain.
E-mail addresses: rafcontr@ucm.es (R. Contreras-Cáceres), lautea@ugr.es (L. Cabeza).

https://doi.org/10.1016/j.ejpb.2023.11.011
Received 6 June 2023; Received in revised form 2 November 2023; Accepted 9 November 2023
Available online 14 November 2023

1. Introduction

In recent years, bioactive compounds extracted from isolated plants have gained significant potential for a successful application in cancer. They have become in an alternative to the above mentioned conventional chemotherapeutic molecules in the sense to being more specific to cancer cells, thus reducing secondary effects. For example, maslinic acid (MA), a pentacyclic triterpene extracted from the olive skin wax, has showed high cytotoxic activity in various types of tumors [1,2]. For instance, in breast cancer, MA induced caspase-independent apoptosis [3], and in CRC it is involved in the induction of apoptosis through the mitochondrial pathway. Moreover, MA has previously been related to the modulation of the expression of cytoskeleton proteins of the HT29 CCR cell line [4,5]. Interestingly, it has been reported that structural modifications of MA or the addition of other molecules improve its biological or solubility capabilities, this offers the possibility to be used in biomedicine in a more extensive manner. In fact, Serbian et al. synthesized acetylated MA derivatives that enhanced the antitumor activity by up to 5-fold in the human lung cancer cell line A549 [6]. Furthermore, Sommerwerk et al. obtained promising results using MA derivatives that increase their antiproliferative activity in some tumor cell lines decreasing their activity in non-tumor NIH 3 T3 mouse fibroblasts [7]. Recently, Fuentes-Ríos et al. synthesized a conjugated tyramine amino acid MA (TMA) with antitumor effect in a wide range of tumor cells, including those of the pancreas, lung, breast, or CRC. Moreover, TMA showed greater antiproliferative activity compared with MA (up to 5-fold) in the human breast cancer cell line MCF-7. In addition, the results in the HCT-15, a CCR cell line characterized by multiresistance mediated through the overexpression of P-glycoprotein, were especially relevant [8].

Breast cancer (BC) and colorectal cancer (CRC) are the first and third most frequent cancers worldwide with 2.3 and 1.9 million new cases per year, causing approximately 700,000 and 900,000 deaths, respectively [9]. However, recent advances in early tumors detection, and the development of new therapeutic strategies against cancer, have considerably improved the prognosis of these patients, thus increasing survival five years after diagnosis [10]. These therapies include surgery (in the case of rejectable tumors), as well as chemotherapy and/or radiotherapy treatments. In this context, some of the commonly prescribed specific active medications for CRC are oxaliplatin, 5-fluorouracil or irinotecan, while for BC are doxorubicin (DOX) or cyclophosphamide, as well as several associations of these drugs. However, an important drawback is that the chemotherapy treatments using these molecules remain severely limited due to its severe toxicity to healthy cells, resulting in serious side effects [11]. Furthermore, about 50 % of patients have tumor recurrence within the first three years after surgical treatment [12]. For these reasons, new cancer treatment strategies are needed to be developed with the aim to release the active drug in a localized and more precise manner. This methodology increases the amount of chemotherapeutic drug in the tumor area with a minimum impact in healthy cells, thus improving the quality of life of cancer patients. Apart from that, the previously mentioned chemotherapeutic compounds possess a high level of cytotoxicity in both cancer and healthy cells. For this reason, apart from the mentioned localized drug delivery, it is also necessary the generation of cytotoxic agents with the capacity to perform their activity only in cancer cells.

Localized drug delivery (LDD), defined as a specific form of targeted delivery where a specific molecule is supplied at a specific area, have been extensively used for the improvement of several interesting researching field, such as cancer treatment [13–15], tissue engineering [16,17], regenerative medicine [18,19] and wound healing [18,20], among other. LDD represent one of the most actual challenges in biomedicine because they are able to locate the drug in a specific and desired area with the aim to be subsequently release in a homogenous, controlled and continuous manner. Among a great number of nanoformulations used for LDD, polymeric nanofibers (NFs) have been extensively reported as nanosystems to encapsulate and release a great variety of chemotherapeutic molecules [21,22]. Indeed, NFs can incorporate numerous molecules and biomolecules, as well as different colloidal nanoparticles acting as nanocarriers, such as mesoporous silica NPs, hydroxyapatite NPs, and liposomes [23–25]. Among various techniques for NFs fabrication, electrospinning is a simple method that produces polymeric NFs in the nanoscale range with large surface area-to-volume ratio, high inter-fiber porosity, low hindrance for mass transfer, flexible handling, adjustable morphology, and well mechanical strength, which make NFs useful as therapeutic patch or mats for drug delivery applications [26,27]. Currently, electrospinning is the most used technique for the incorporation of chemotherapeutic molecules, or biomolecules into NFs to be used in a controlled administration process [28–31]. Moreover, electrospinning is also used for the incorporation of several nanoparticulated systems [13], such as micelles [32], vesicles [33], silica particles [34], metal nanoparticles [35–37], magnetic nanoparticles [38,39], carbon nanotubes [40,41], or TiO_2 nanoparticles [42,43]. In electrospinning, when a strong electrostatic field is applied to a polymer solution held in a syringe, the pendent droplet of the polymer solution from the capillary outlet is deformed into the denoted as Taylor cone [44]. When the electric force overcomes the surface tension of the droplet, one or multiple charged jets are ejected from the tip of the droplet. As the jet moves towards a collecting metal screen the solvent evaporates, and a nonwoven fabric mat is formed on the screen (see Fig. 2). Indeed, apart from electrospinning, there are other available methods and procedure to produce polymeric nanofiber with the capability to encapsulate bioactive molecules and nanosystems for drug delivery applications [45]. For example polymeric nanofibers were prepared through a peptide amphiphile (PA)-based self-assembling system [46]. PAs consisted on a dialkyl chain moiety (hydrophobic component/tail group) attached to an N-alpha amino group of a peptide chain (hydrophilic component/head group), resulting on a “peptide amphiphile”. Another method to fabricate polymeric nanofibrous materials is through a technique called thermally induced liquid–liquid phase separation [47]. This technique involves five basic steps: *i)* dissolution of polymer, *ii)* liquid–liquid phase separation process, *iii)* polymer gelation, *iv)* extraction of solvent from the gel with water and *v)* freezing and freeze-drying under vacuum. Apart from that, conventional polyaniline synthesis is known to produce particulate products with irregular shapes by introducing “structural directing agents” during the chemical polymerizing reaction [48]. More recently, metal–organic framework (MOF) nanostructures have been used to obtain nanomaterials with desirable features, such as polymeric nanofibers [49]. MOFs consist of metal ions and organic linkers that are assembled in different geometries and can be produced in 1, 2, or 3 dimensions. Polylactic (PLA)/cellulose nanofibers (CNFs) have been also prepared by a procedure involving solution casting and direct melt mixing [50]. CNFs have demonstrated excellent properties for biomedical applications. This system can be prepared by dissolving PLA pellets into a solution containing CNFs. This mixture is melted through vacuum pump and introduced into an oven at specific conditions. Finally, nanofibers can also be prepared by melt extrusion of immiscible blends via in situ formation of microfibrils during a melt extrusion process [51].

Specifically for drug release, numerous polymers are used for the fabrication of nanofibers, such as polylactic acid (PLA), poly lactic-co-glycolic acid (PLGA), polyethylene glycol (PEG), polyethylene oxide (PEO) or polycaprolactone (PCL) [20,52–54]. Specifically, electrospun PLA and PCL mats are widely investigated, both polymers are approved by Food and Drug Administration (FDA), and are of the most favorable materials with better biocompatibility, biodegradability, high mechanical strength and sustained biodegradation [13,55,56].

In this work, a comprehensive in vitro comparative analysis is initially performed between MA and the tyramine-derivative (TMA) (Fig. 1). The assays include cell cycle analysis, genotoxicity, angiogenesis and apoptosis tests based on previous results obtained, where we observed an evident improvement in antiproliferative activity with TMA

treatment compared with MA in pancreatic, breast, lung and brain cancer cell lines [8]. The improved antitumor activity of the TMA was confirmed, and then, it was incorporated as a new system based in drug-loaded electrospun NFs to exploit the cytotoxicity activity in colon and breast cancer cell lines. In this sense, we have synthetized the drug-loaded polymeric NFs to be applied as local cancer therapy. In specific, TMA was incorporated into PLA, PCL and PLA/PVP NFs by the electrospinning technique. Finally, the cytotoxicity analysis of TMA-loaded NFs demonstrated that there was a significant reduction of cell proliferation in the cell lines tested. Our results suggest that our electrospun NFs system may represent an advance to improve the local treatment of colon cancer by loading a TMA derivative with a better antitumor effect than its predecessor, MA.

2. Materials and methods

2.1. Materials

Poly(lactic acid) (PLA 4060D) was supplied by Doxa Microfluidics. Polycaprolactone (PCL) (Mw = 80.000), phosphate buffered saline tablets and the solvents ethanol 70 %, 1,4-dioxane, dichloromethane (DCM) and dimethylformamide (DMF) were purchased from Merck (Darmstadt, Germany) and used without further purification. Water was purified using a Milli-Q system (Millipore, Burlington, MA, USA).

2.2. Cell culture

The tumor cell lines of MCF-7 (human breast cancer), T84 (human colon adenocarcinoma), SF-268 (human glioblastoma), PANC-1 (human pancreatic adenocarcinoma), A549 (human lung cancer), B16-F10 (murine melanoma) and L929 (murine fibroblast) were provided by the Centre for Scientific Instrumentation of the University of Granada (CIC-UGR, Spain). All cell lines were grown in Dulbecco's Modified Eagle's Medium (DMEM) (Sigma-Aldrich, Madrid, Spain) supplemented with 10 % fetal bovine serum (FBS) and 1 % of penicillin–streptomycin (Sigma–Aldrich, Madrid, Spain) and maintained at 37 °C in a humidified atmosphere with 5 % CO_2.

2.3. Cell cycle analysis

T84, MCF-7, SF-268, PANC-1, A549, B16-F10 and L929 were seeded in 12-well plates at a density of 5×10^4 cells/well for T84, SF-268, PANC-1, A549 and L929, and 3.75×10^4 cells/well for MCF-7, and 2.5×10^4 for B16-F10 cells/well. Cell lines were provided by the Centre for Scientific Instrumentation of the University of Granada (CIC-UGR, Spain) and maintained in the same culture conditions of the rest of cell lines. After 8 h, the culture medium was replaced with serum-free culture medium to synchronise the cell cycle and incubated overnight. Then, the culture medium was replaced with fresh supplemented DMEM containing MA and TMA at a half-maximal inhibitory concentration (IC_{50}) previously obtained by our group for T84 and MCF-7 cell lines [8]. After 48 h of incubation, cells were trypsinized, centrifugated and fixed with cold 70 % ethanol for 30 min at 4 °C. Later, cells were centrifuged, washed twice with PBS, and incubated with PI/RNAse Solution (Immunostep, Salamanca, Spain). Finally, samples were analysed by FACScan flow cytometer (Becton Dickinson, San Jose, CA, USA) using FlowJo software (Treestar, Ashland, OR, USA).

2.4. Genotoxicity, angiogenesis and apoptosis tests

2.4.1. Comet assay

Cell lines were seeded in 48-well plates at a density of 1×10^4 cells/well for T84 and 3×10^3 cells/well for MCF-7 and were treated at IC_{50} dose with MA, TMA, for 48 h and hydrogen peroxide overnight as positive control. Then, cells were trypsinized, centrifuged and resuspended in 100 μL of 0.75 % low gelling temperature agarose (Sigma-Aldrich, Madrid, Spain) dissolved in PBS at 37 °C. The cells were placed onto microscope slides previously coated with a thin layer of 1 % agarose (Sigma-Aldrich, Madrid, Spain) dissolved in milliQ water. After and incubation at 4 °C for 1 h, the samples were lysed (2.5 M NaCl, 100 mM EDTA, 10 mM Tris and 1 % Triton X-100, pH 10) during 1 h at 4 °C. After that, the samples were transferred into cold alkaline solution (300 mM NaOH and 1 mM EDTA, pH 13) for 20 min and then, an alkaline electrophoresis was carried out in electrophoresis solution (30 mM NaOH and 1 mM EDTA, pH 13) during 20 min at 73 V, 300 mA at 4 °C [57]. Finally, the samples were washes three times in 0.4 M Tris pH 7.5, fixed with absolute ethanol for 10 min and left to dry and then they were stained with Hoechst 33,258 solution (1 μg/mL) (Sigma-Aldrich,

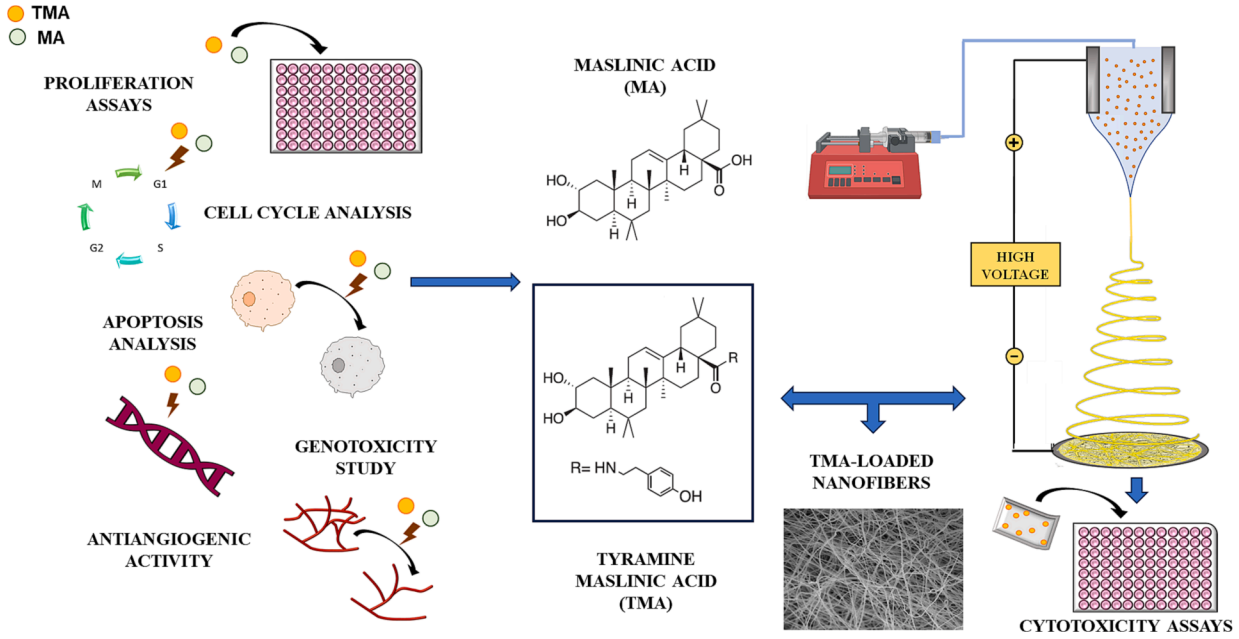

Fig. 1. Schematic representation of the antitumor assays and the drug-loaded polymeric nanofibers fabrication.

Madrid, Spain) for 5 min and examined under a fluorescence microscope Leica DM IL LED (Leica Microsystems, Wetzlar, Germany). A minimum of 50 randomly cells/slide were analyzed using the open-source software OpenComet v1.3.1. The relative proportion of DNA damage in tail (Tail DNA %) was established to assign comets into five categories: Score 0 (<5% = no damage), Score 1 (5–20 % = low damage), Score 2 (20–40 % = moderate damage), Score 3 (>40–80 % = high damage), and Score 4 (≥80 % = extreme damage) [58].

2.4.2. Western blot analysis

T84 and MCF-7 cells were seeded in T75 culture flasks (Thermo Scientific, Waltham, MA, USA) at a density of 1.5×10^6 and 5×10^5 cells/flask, respectively. Cells were exposed to IC_{50} values of MA, TMA for 48 h and hydrogen peroxide overnight (positive control). After the incubation times, cells were collected, centrifuged, and total proteins were extracted with RIPA lysis buffer (Sigma-Aldrich, Madrid, Spain), with 1 % Halt™ Phosphatase Inhibitor Cocktail (Thermo Scientific, Waltham, MA, USA) and 1 % Protease Inhibitor Cocktail (Sigma-Aldrich, Madrid, Spain) to determine protein concentration using Bradford assay (Sigma-Aldrich, Madrid, Spain). For each sample, 40 μg of protein were heated during 5 min at 95 °C and separated by electrophoresis in 12 % SDS-PAGE gel for histone H2AX and caspase 8 and 10 % SDS-PAGE gel for VEGFA and PARP-1, all in a Mini Protean II cell (Bio-Rad, Hercules, CA, USA). Proteins were transferred to a nitrocellulose membrane (45 μm pore size) (Millipore, Burlington, MA, USA) at 20 V for 1.5 h and blocked in Phosphate-Buffered Saline (PBS)-0.1 % Tween-20 + 5 % (w/v) milk powder for all proteins except histone H2AX and caspase 8 for which 5 % BSA in Tris-Buffered Saline (TBS)-0.1 % Tween-20 was used for 1 h under stirring. After three washes with washing solution, the membranes were incubated overnight at 4 °C with the primary antibodies: Phospho-Histone H2A.X (MA1-2022) Monoclonal Antibody (1:1000) (Thermo Scientific, Waltham, MA, USA), Anti-PARP1 [E102] Antibody (ab32138) (1:2000) (Abcam®, Cambridge, UK), Caspase 8 Monoclonal Antibody (90A992) (1:1000) (Thermo Scientific, Waltham, MA, USA) and Anti-VEGFA Polyclonal Antibody (ab46154) (1:1000) (Abcam®, Cambridge, UK) After three washes with washing solution, the membranes were incubated for 1 h with the secondary antibody m-IgGκ BP-HRP (sc-516102) (1:2000) and Mouse anti-rabbit IgG-HRP (sc-2357) (1:5000) (Santa Cruz Biothecnology, CA, USA) at room temperature and revealed by chemiluminescence (Amersham Biosciences, Saint Louis, MO, USA), using the mouse monoclonal anti-β-actin – peroxidase antibody (A3854) (1:25000) (Sigma-Aldrich, Madrid, Spain) as an internal control. The images obtained were analyzed using Quantity One analytical software (Bio-Rad, Hercules, CA, USA).

2.4.3. Apoptosis detection via Annexin V-FITC/PI assay

T84 and MCF-7 cells were seeded in 6-well plates at a density of 1×10^5 cells/well for T84 and 8×10^5 cells/well for MCF-7 while L929 cells were seeded in 12-well plates at a density of 5×10^4 cells/well. After 24 h, cells were treated with IC_{50} doses of MA and TMA. After 48 h of treatment cells were trypsinized, centrifugated and washed with PBS. Later, cells were resuspended in 1X Annexin binding buffer and incubated in darkness for 15 min with annexin V-FITC and PI as indicated in the FITC Annexin V Apoptosis Detection Kit with PI (Immunostep, Salamanca, Spain). Finally, 200 μL of 1X Annexin binding buffer was added, and samples were analysed by FACScan flow cytometer (Becton Dickinson, San Jose, CA, USA) using FlowJo software (Treestar, Ashland, OR, USA).

2.5. Fabrication of polymeric nanofibers and TMA-loaded polymeric nanofibers

The electrospinning experimental setup used for the fabrication of pure PLA and PLA/HE NFs is included in Figure S1. Nanofibers were obtained at atmospheric pressure and room temperature. This device is divided in the syringe pumps, the injector, two high voltage suppliers to generate the Taylor cone, and the collector. For the synthesis of pure NFs, a specific amount of polymer (PLA or PC) or mixture polymer (PLA/PVP) were added to a mixture of 1,4-dioxane, DMF, DCM or EtOH (see Table 1 for details), and they were magnetically stirred during 12 h at room temperature in each case. Then, each polymeric solution was collected in a plastic syringe, and it was pumped through a metallic

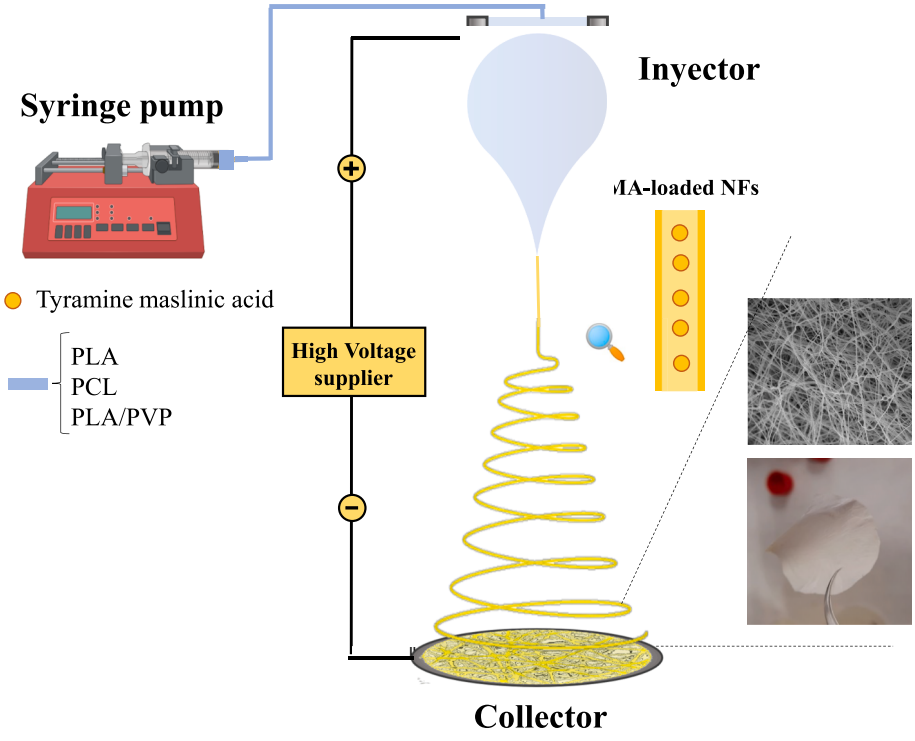

Fig. 2. Schematic representation for the fabrication of the PLA/HE NFs by electrospinning.

needle (outer diameter 0.9 mm and inner diameter 0.6 mm) through a PTFE capillary (outer diameter 1.6 mm, inner diameter 0.8 mm) at a flow rate between 0.5 and 0.7 mL/h. To generate the Taylor cone, the solution was sprayed at voltage between 15.5 and 17.2 kV, being the sum of two voltages suppliers. The positive electrode was connected to the injector and the negative electrode was connected to the collector, which consisted of a stainless-steel flat platform covered with aluminum foil, which was placed at 15 cm from the tip of the needle (see Figure S1 for details). A typical fabricated electrospun mat was about 15 cm diameter when removed from the collector. Finally, the presence of residual solvents and free drug in the fabricated NFs was eliminated in a vacuum oven during 24 h at room temperature. For incorporation of TMA into the polymeric NFs 50 mg of the previously obtained maslinic acid derivative was added to each solvent mixture before the addition of the polymer. After that, the same parameters followed for the fabrication of the pure polymeric NFs during the electrospinning process were used to obtain TMA-loaded NFs.

2.6. Characterization

The size and fiber distribution of the electrospun NFs were visualized by using a scanning electron microscope (SEM, JEOL JSM 6335F, Tokyo, Japan) working at 15 KV. Samples were previously sputtered with gold to minimize charging effect. The fiber diameter was measured from the SEM image by analyzing at least 50 different fiber segments whose diameters were measured using ImageJ software.

2.7. Encapsulation efficiency

The efficiency of TMA encapsulation in NFs was calculated by high performance liquid chromatography (HPLC). Briefly, 1 mg of each NF was dissolved in 1 mL of acetonitrile and injected in HPLC with a previous optimized method. A C18 column (250 x 4.6 mm, 5 μm, Gemini) was used with a flow rate of 1 mL/min and a column temperature of 25 °C. The mobile phase was acetonitrile:water (80:20, v/v) with 0.1 % of trifluoroacetic acid; the determine wavelength was 210 nm and the elution time was about 6 min. A calibration curve was previously prepared for the determination of TMA concentration.

2.8. Drug release assay

TMA-loaded NFs (1.5 mg each, 3 % TMA) were suspended in phosphate buffered saline solution (PBS, 2 mL, pH = 7.5) in 3 mL glass vials. The tubes were placed in a water bath at 37 °C, with mechanical shaking at 100 rpm. At specific intervals (0–48 h), the release medium containing the drug was transferred out to a UV quartz cell, and UV absorption was measured (227 nm). Fresh release medium (PBS, 2 mL) was added to the test tube for the cumulative-release studies. Similarly, for continuous-release measurements, TMA-NFs (1.5 mg each) were suspended in phosphate buffered saline (PBS, 2 mL, pH = 7.5) in UV quartz cell at 37 °C, and UV absorption was measured (227 nm) at specific intervals (0–48 h).

Table 1
Amount of polymer and solvent used for the fabrication of pure and TMA-loaded NFs. The amount of TMA is also included.

Sample	Polymer/ g	Dioxane/ mL	DMF/ mL	DCM/ mL	EtOH/ mg	MA/ mg
PLA	1.7	4.7	3.60	–	–	–
TMA-PLA	1.7	4.7	3.60	–	–	51
PCL	1.9	–	3.8	3.1	–	–
TMA-PCL	1.9	4.56	3.8	3.1	–	51
PLA/PVP	1.2/0.6	3.2	2.7	–	2.5	–
TMA-PLA/PVP	1.2/0.6	3.2	2.7	–	2.5	51

2.9. Degradation study

A total of 24 mg of TMA-NFs was added to Dulbecco's Modified Eagle's Medium (DMEM) (Sigma-Aldrich, Madrid, Spain) and incubated for 9 days at 37 °C in a humidified atmosphere with 5 % CO_2 (simulating cell culture conditions). After that, the NFs were air-dried and weighed. The degradation of the NFs was calculated as the difference between the initial and final weight.

2.10. Cell viability assay

To test TMA-loaded NFs proliferation effect, T84, MCF-7 and L929 cells were seeded in 96-well plates at a density of 2×10^3, 7×10^2, and 4×10^3 cells/well respectively, with 200 μL of culture medium. To test the proliferation effect of free drugs in a no-tumor cell line, L929 cells were seeded in 48-well plates at a density of 8×10^3 cells/well in 300 μL of culture medium. After 24 h, L929 cells in 48-well plates were treated with an increasing range of concentrations from 1 to 80 μg/ml of MA and TMA. At the same time, T84 and MCF-7 cells in 96 well plates were treated with, 0.47 mg of 3 % TMA-loaded PLA/PVP NFs, 3 % TMA-loaded PCL NFs, PLA/PVP NFs, PCL NFs and an equivalent concentration of free TMA. After 48 h of incubation, the percentages of proliferation of treated cells were obtained by the modified colorimetric assay of sulforhodamine B (SRB) (Sigma-Aldrich, Madrid, Spain), for which 10 % trichloroacetic acid (TCA) (Sigma-Aldrich, Madrid, Spain) was applied as cell fixative for 20 min at 4 °C. After that, 0.4 % SRB diluted in 1 % acetic acid was used during 20 min in agitation and at room temperature to stain cells. Finally, Trizma® (10 mM, pH 10.5) (Sigma-Aldrich, Madrid, Spain) was employed for solubilize SRB and the optical density (OD) was evaluated at 492 nm in a spectrophotometer EX-Thermo Multiskan (Waltham, Massachusetts, USA) [59].

2.11. Statistical analyses

All the results were expressed as the mean ± standard deviation (SD). Statistical analysis was performed using Student's t-tests and Kruskal-Wallis tests with the Statistical Package for the Social Sciences (SPSS) v.26 software with a significance level of $\alpha = 5$ %.

3. Results and discussion

3.1. Proliferation assay

Our previous results showed a stronger IC_{50} reduction with TMA treatment compared with MA in cell lines of different types of cancer including T84, HCT-15, MC38, MCF-7, MDA-MB-231, A549, H520, A172, SF-268, PANC-1, MIA PaCa-2 and B16-F10 (2.37, 2.07, 2.06, 4.12, 1.82, 1.99, 1.78, 1.86, 3.00, 2.54, 2.82, and 4.72 times that TMA reduces MA IC_{50} in cell lines respectively) [8]. In this work we tested MA and TMA in the no tumor mouse fibroblast L929, TMA showed significant differences at all doses tested compared with MA ($p < 0.05$) (Figure S2). In addition, in T84 CRC and MCF-7 BC cell lines, the reduction of the IC_{50} value was 2.37 and 4.12 times, respectively, similar to the results obtained for the fibroblast L929. At 60 μg/mL and below, MA was significantly less cytotoxic than TMA ($p < 0.05$) with MA IC_{50} value of 45.31 ± 1.91 μg/mL and TMA IC_{50} of 20.45 ± 1.91 μg/mL (2.22-fold reduction). This could indicate that both MA and TMA act through a common mechanism, in both tumor and non-tumor cells, since MA and urea derivatives had been previously tested in another murine fibroblast cell line (NIH 3 T3), obtaining a similar cytotoxicity results [60]. In addition, the synthesis of the derivative may change the chemical nature of drug and could affect its cytotoxic mechanism of action and selectivity towards non-tumor cells. Thus, the chemical modifications of the drug

could improve cytotoxicity but not selectivity towards non-tumor cells [61]. Although this fact could be considered a challenge for possible in vivo assays, the biocompatibility of other triterpenes has already been reported. Interesting, a benzylamide conjugate of MA has been shown to have good compatibility with the chorioallantoic membrane (CAM) without alterations of the stages of development [62].

3.2. Cell cycle analysis

The modulation of cell cycle from a wide range of solid tumor cell lines treated with MA and TMA were studied. In all tumor cell lines, MA and TMA significantly reduced the percentage of cells in S and G2/M phases compared to untreated cells ($p < 0.05$) (Fig. 3 and S3). Interestingly, TMA showed a significant higher cell percentage in the G0/G1 phase in T84, A549 and SF-268 cells (18.1 % in SF-268 cells) compared to MA ($p < 0.05$). In contrast, the increase in percentage of cells in subG1 phase was significantly lower than in MA in T84 and SF-268 cells, up to 21.9 % decrease in SF-268 cell line ($p < 0.01$). In the non-tumor cell line L929, MA did not alter the cell cycle compared to the control but significantly increased the percentage of cells in subG1 phase ($p < 0.05$). However, TMA modified all phases of the cell cycle ($p < 0.05$) and reduced subG1 and G2/M phases compared to MA (7.8 % and 2.3 %, respectively) ($p < 0.05$). Our results suggest that MA could be involved in the modulation of cell cycle of different tumor cell lines, with higher cell percentage in G0/G1 phase and a consequent decrease in the S phase. MA could downregulate the ERK pathway, implicated with cell cycle proteins required for the transition from G1 phase to S phase [3,63]. Besides, tyramine may alter the expression of genes related to the response to DNA damage causing by the genotoxicity of the amino acid, which could lead to an alteration of the cell cycle [64]. Furthermore, these differences found in the cell cycle are in agreement with previous results reported for other MA derivatives [60,65,66].

3.3. Genotoxicity study of TMA and MA

The treatment of T84 and MCF7 cells with hydrogen peroxide as well as with MA and TMA resulted in significant DNA damage by the production of comets in the treated cells (Fig. 4). All comet characteristics were modified by exposure to MA, TMA and hydrogen peroxide in both cell lines (Table 2). In T84 cell line, all comet characteristics showed significant differences between MA and TMA ($p < 0.001$), except comet head length, while in MCF-7 cells these differences were observed in all comet characteristics ($p < 0.05$), except comet head intensity and the relative proportion of DNA in tail. Thus, in general TMA was less genotoxic than MA. Furthermore, T84 cells showed a 12 % significant decrease in the relative proportion of DNA in tail with de treatment of TMA ($p < 0.001$) compared with MA, while no statistically significant differences were found in MCF-7 cell line (Fig. 4A). This parameter was

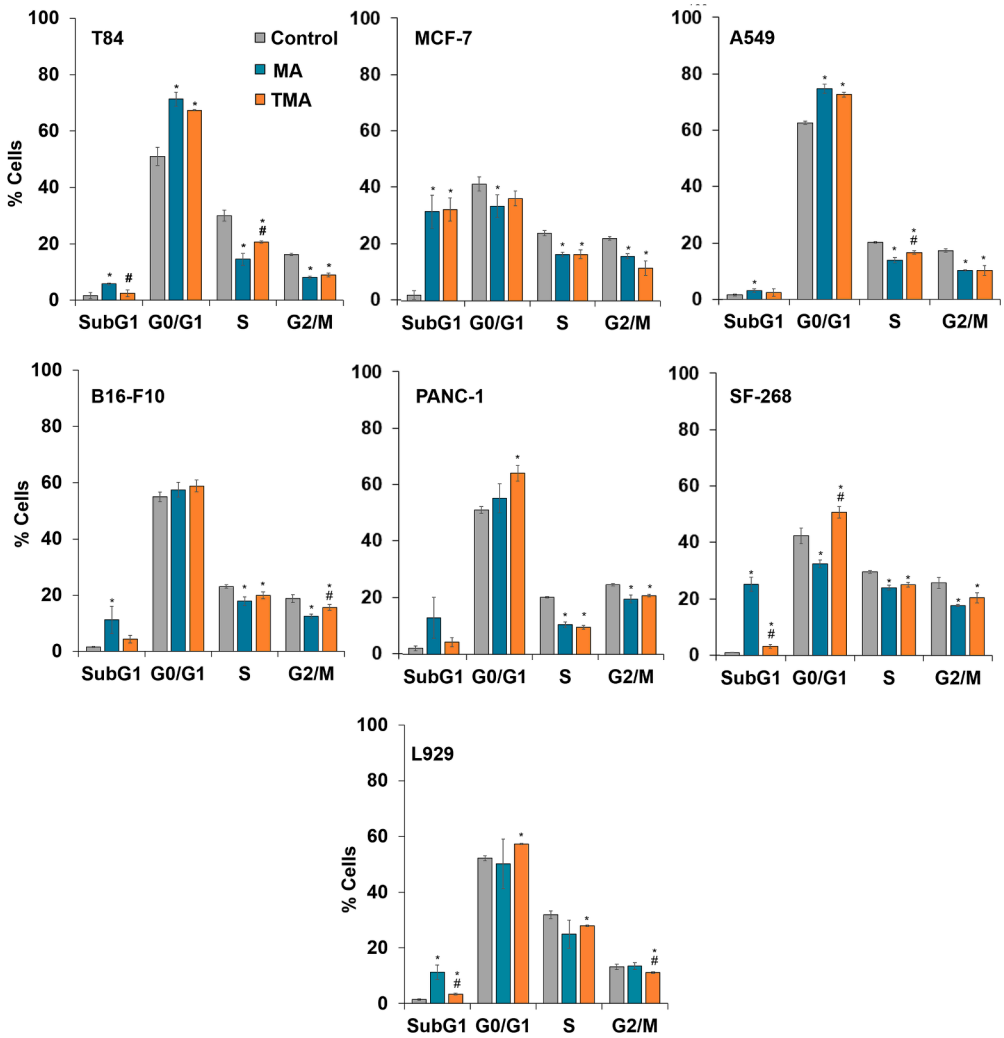

Fig. 3. Modulation of cell cycle by MA and TMA. Tumor T84, MCF-7, A549, B16-F10, PANC-1 and SF-268 cell lines were exposed to IC_{50} doses of the two drugs for 48 h. Untreated cells were used as negative controls. In addition, cell cycle of normal L929 was assayed. Data were represented as the mean value ± standard deviation of triplicate cultures. (*) $p < 0.05$ compared with untreated control. (#) $p < 0.05$ compared with MA.

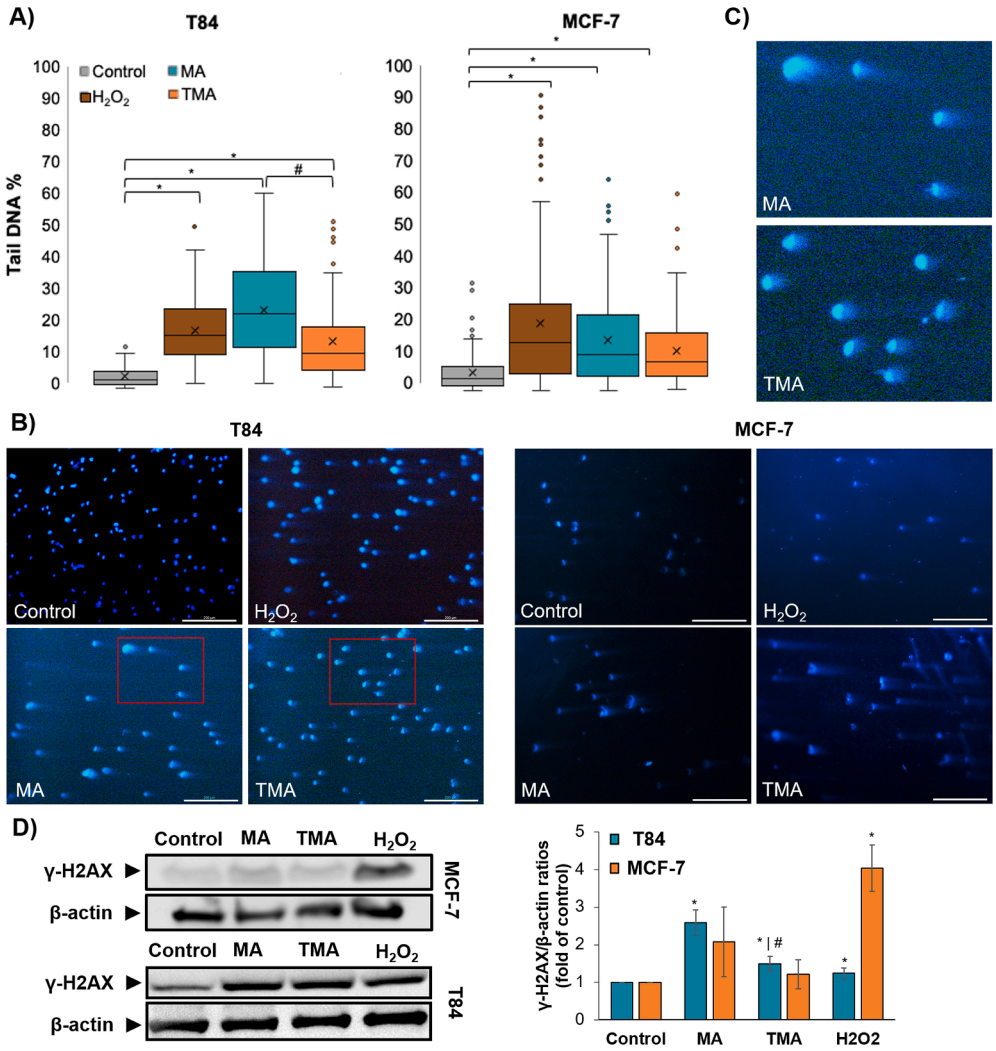

Fig. 4. Genotoxicity study. **A.** DNA damage response to exposure to MA, TMA and hydrogen peroxide in T84 and MCF-7 cells lines. Hydrogen peroxide (H_2O_2) was used as positive control. Distribution of the relative proportion of DNA in tail in comets ($n = 110$ for each treatment). **B.** Comet images of the cells lines stained with Hoechst 33258 solution. **C.** Zoomed-in details of the squares marked in red (**C**). Scale bar = 200 μm. D. Phosphorylation of histone H2AX (γH2AX) after exposure to MA, TMA and hydrogen peroxide in T84 and MCF-7 cell lines·H_2O_2 was used as positive control. Western blot images of γH2AX in both cell lines. β-actin was used to normalise protein expression. The figure shows a graphic representation of western blot densitometry analysis of bands corresponding to coefficient between γH2AX and β-actin expression. (*) $p < 0.05$ compared with negative control. (#) $p < 0.05$ compared with MA. (For interpretation of the references to colour in this figure legend, the reader is referred to the web version of this article.)

applied to assign scores to each comet (Table 3). In fact, in both cell lines the negative control had a low DNA damage with comet population mostly distributed in scores 0 and 1, and TMA showed low DNA damage with scores 0, 1 and 2. However, MA had higher DNA damage than TMA and negative control with a percentage of comets classified in score 3.

In the western blot analysis of γH2AX, all the treatments showed an increased in γH2AX compared with the negative control both in T84 and MCF-7 cells ($p < 0.05$) (Fig. 4D). Furthermore, the histone phosphorylation was 1.7-fold lower with the treatment of TMA compared with cells treated with MA in both cell lines, correlating with less DNA damage and consequently decreased genotoxicity.

DNA damage may cause cell death or cell cycle arrest. For this reason, comet assay and the analysis of the histone H2AX phosphorylation (γH2AX) were carried out in MCF-7 and T84 cell lines. Comet assay has been widely used as quantification method to determine DNA damage in generic terms while DNA double-strand breaks result in a rapid phosphorylation of H2AX, making it a very sensitive and used marker to identify genotoxic drugs [67–69].We found that MA has a genotoxic effect on the CRC cell line T84 and the BC cells MCF-7 which is in accordance with previous results with CRC and human cervical cancer and could be related with the induction of mitochondrial intrinsic pathway involving the activation of c-Jun NH_2-terminal kinase (JNK) and the subsequent p53 induction, leading to a possible caspase 8-independent cell death pathway [3,4,60,70,71]. In both assays TMA induced significantly lower DNA damage and, therefore, was less genotoxic than MA, suggesting that, although TMA exhibits enhanced cytotoxicity, this may not be a consequence of increased DNA damage.

3.4. Antiangiogenic activity

For the analysis of the antiangiogenic effect of MA and TMA, western blot analyses to determine the expression of vascular endothelial growth factor A (VEGFA) protein were carried out in T84 and MCF-7 cell lines. Both drugs produced a significant reduction in the expression of VEGFA in MCF-7 cells of 1.32 and 2.12-fold for MA and TMA ($p < 0.05$) treatments respectively compared with no treated cells. However, in T84 cell line the expression of VEGFA seems to be not modified. No significant variations were found between both treatments (Fig. 5A).

A potentially promising target for cancer treatment could involve angiogenesis, since increased tumor angiogenesis has been associated

Table 2
Effect of MA and TMA on comet characteristics in T84 and MCF-7 cells. Hydrogen peroxide was used as positive control. Data were represented as mean or median of 110 comets for each treatment of duplicate experiences. (***) $p < 0.001$ compared with the negative control. (###) $p < 0.001$ compared with MA.

T84				
Comet characteristics	**Negative control ($n = 110$)**	**Positive control ($n = 110$)**	**MA ($n = 110$)**	**TMA ($n = 110$)**
Head lengthMean ± SD	61.78 ± 13.18	68.98 ± 12.64 ***	69.02 ± 14.52 ***	64.85 ± 16.29
Head intensity Mean ± SD	131.91 ± 32.56	89.53 ± 30.25 ***	51.66 ± 28.45 ***	79.16 ± 30.54 *** | ###
Tail length Medianmin - max	0(0 – 16)	22.5 ***(0 – 79)	30 ***(0—95)	13 *** | ###(0 – 71)
Tail moment Medianmin - max	0(0 – 2.18)	4.57 ***(0 – 41.02)	7.68 ***(0 – 43.89)	1.61 *** | ###(0 – 33.55)
Olive moment Medianmin - max	0.28(0 – 3.96)	6.17 ***(0.16 – 22.85)	9.30 ***(0.04 – 30.03)	3.64 *** | ###(0—22.20)
Tail DNA % Median (min – max)	2.94(0.36 – 14.11)	16.95 ***(1.89 – 51.93)	23.96 ***(1.94 – 62.35)	11.23 *** | ###(0.60 – 54.03)
MCF-7				
Comet characteristics	**Negative control ($n = 110$)**	**Positive control ($n = 110$)**	**MA ($n = 110$)**	**TMA ($n = 110$)**
Head lengthMean ± SD	69.56 ± 16.74	79.33 ± 31.45 *	78.10 ± 28.43	67.04 ± 29.68 #
Head intensity Mean ± SD	88.90 ± 37.76	55.94 ± 36.85 *	59.61 ± 35.30 *	58.57 ± 35.39 *
Tail length Medianmin - max	0(0 – 27)	33.5 *(0 – 295)	29 * (0—171)	6.5 * | #(0 – 266)
Tail moment Medianmin - max	0(0 – 8.61)	5.40 *(0 – 235.34)	2.93 *(0 – 96.90)	0.42 * | #(0 – 165.64)
Olive moment Medianmin - max	0.48(0 – 9.25)	7.06 *(0 – 79.67)	3.96 *(0 – 37.97)	1.74 * | #(0 – 39.85)
Tail DNA % Median (min – max)	3.70(0.05 – 34.07)	15.07 * (0.01 – 93.73)	11.53 * (0.09 – 67.14)	9.11 *(0.15 – 62.27)

Table 3
Distribution of comet percentages in T84 and MCF-7 cells in the established scores according to the relative proportion of DNA in tail. Cells were exposed to MA, and TMA. Cells treated with hydrogen peroxide were used as positive control. Score 0 (<5% Tail DNA %), Score 1 (5–20 % Tail DNA %), Score 2 (20–40 % Tail DNA %), Score 3 (>40–80 % Tail DNA %) and Score 4 (≥80 % Tail DNA %).

T84					
Treatment	**Score 0 (% Comets)**	**Score 1 (% Comets)**	**Score 2 (% Comets)**	**Score 3 (% Comets)**	**Score 4 (% Comets)**
Control	71	29	0	0	0
H_2O_2	9	46	40	5	0
MA	9	32	39	20	0
TMA	18	57	17	7	0
MCF7					
Treatment	**Score 0 (% Comets)**	**Score 1 (% Comets)**	**Score 2 (% Comets)**	**Score 3 (% Comets)**	**Score 4 (% Comets)**
Control	59	38	3	0	0
H_2O_2	24	37	25	12	3
MA	31	37	24	8	0
TMA	33	45	20	3	0

with enhanced tumor aggressiveness. Thus, chemotherapeutic drugs which decrease angiogenesis activity in tumors could be a good strategy in cancer therapy. It has recently been observed that the cytokine VEGFA play an important role in the formation of vessels in tumors [72]. The decrease of VEGFA levels was described in previous studies in which MA treatment and was associated with a reduction in tumor angiogenesis and a lower expression of VEGFA [73–75]. Our derivative with tyramine maintained this anti-angiogenic effect and although not significantly, could increase it.

3.5. Apoptosis analysis

A possible cell death via apoptosis produced by MA and TMA was studied by western blot analysis of the expression of caspase 8 and poly (ADP-ribose) polymerase 1 (PARP-1) and by flow cytometry by FITC Annexin V with PI. The exposure to MA and TMA had no significant effect on caspase 8 expression in MCF-7 cells while in T84 cells a significant reduction in the expression of caspase 8 and cleaved caspase 8 of 1.42 and 2.07-fold, respectively ($p < 0.01$) (Fig. 5A) was observed. In addition, both MA and TMA resulted in a significant downregulation of full length PARP-1 expression (116 kDa), with a reduction of 1.77-folds of full length PARP-1 in T84 cells treated with TMA compared with MA ($p < 0.05$), which could suggest a possible activation of the protein. Concerning apoptosis detection by FITC Annexin V with PI, in both tumor cell lines T84 and MCF-7, MA showed an increase in the percentage of necrotic cells of 1.6 % and 3.5 % compared with control cells, respectively, while in T84 cells treated with TMA this increase disappeared ($p < 0.05$) (Fig. 5B and S4). Meanwhile, TMA resulted in a significant increase in apoptosis in T84 and MCF-7 tumor cells, in the percentages of cells in both early and late apoptosis ($p < 0.05$). Of particular interest is the rise of cells in early apoptosis in MCF-7 cell line of 14.2 % concerning untreated cells ($p < 0.001$). Interestingly, this effect has not been observed in no-tumor cells L929, in which TMA produced a significant decrease in the percentage of cells in early apoptosis, 5.9 % less than MA ($p < 0.01$).

Previous studies have described some mechanisms of action of MA to explain its antitumor effect, such as the inhibition of NF-κB, or the induction of autophagic pathway via downregulation of autophagy related proteins in pancreatic cancer cell lines [2,73]. However, TMA could triggers cell death by a possible different pathway to MA, such as parthanatos [76]. Furthermore, caspase 8 modulate cell death by apoptosis or necroptosis, and its inhibition would be related to necroptosis through the activation of proteins such as receptor-interacting serine-threonine protein kinase [77,78].Our results suggest that TMA could induced an increase in a possible caspase-independent apoptosis in both tumor cell lines and PARP-1 activation in T84 cell line compared to MA, supporting data obtained for other MA derivatives [60,79,80]. Interestingly, TMA induced low early apoptosis in the non-tumor murine fibroblast line L929 compared to MA, which could be related with the reduction of cell percentage in subG1 and G2/M phases compared to MA and less genotoxicity suggesting a possible reduction in normal tissue injury.

3.6. Synthesis and characterization of NFs and TMA-loaded NFs

Initially, PLA and PCL NFs were fabricated by the electrospinning technique, and then, due to its biocompatibility and biodegradability, they were used for the incorporation of TMA. The percentage of PLA was adjusted at 17 %, which produced nanofibers with total absence of beads, and it was dissolved in a mixture of 1,4-dioxane and DMF (see experimental section for details). The amount of PCL was also adjusted at 19 %, which was dissolved in a mixture of DCM and DMF (see experimental section for details). For the fabrication of the drug loaded NFs (TMA-NFs), the amount of TMA was 3 %, with respect to the amount

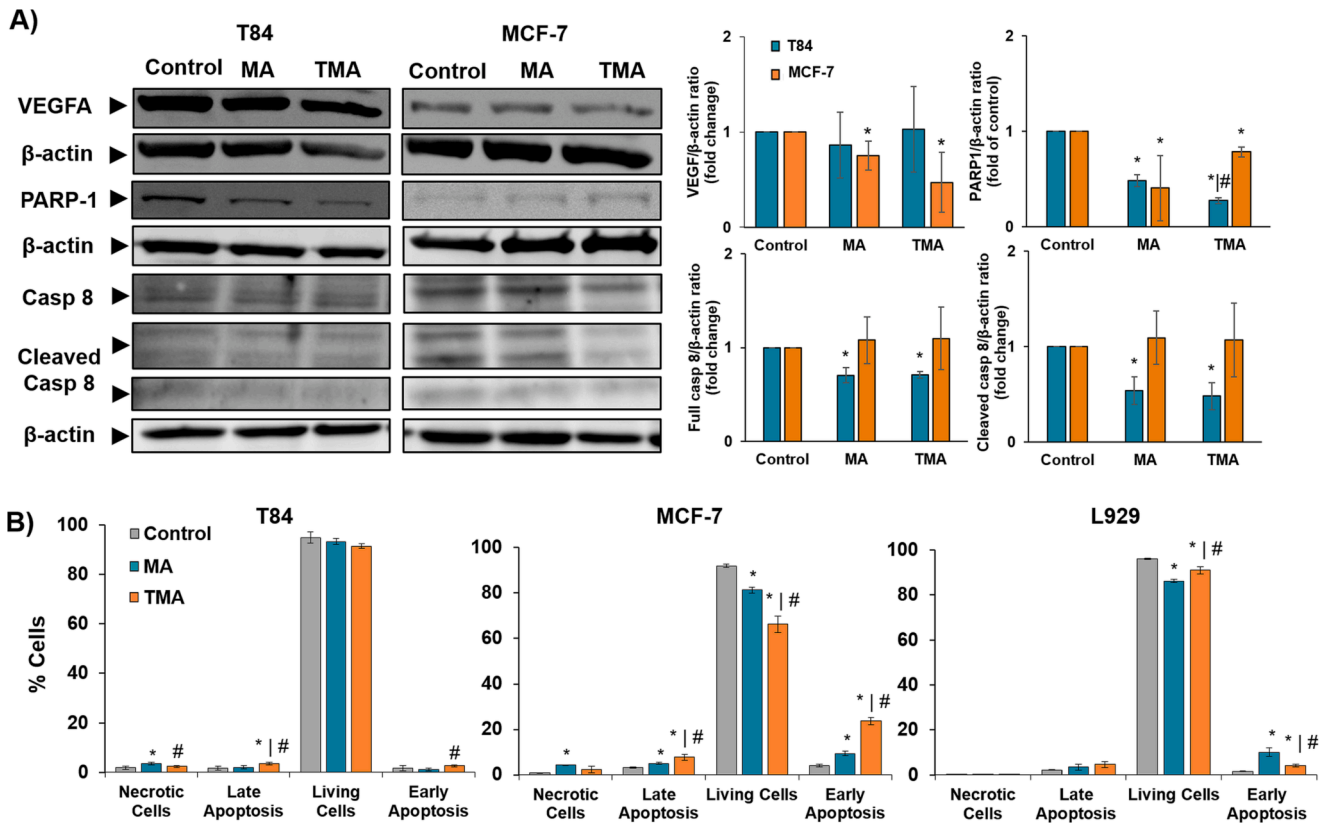

Fig. 5. Antiangiogenic and apoptosis activity. **A**. Western blot images and densitometry analysis of bands corresponding to coefficient between protein and β-actin expression of expression of the VEGFA, caspase 8 and PARP-1. β-actin was used to normalise protein expression. Results are shown as mean ± S.D. of duplicate cultures. (*) $p < 0.05$ compared with control cells. (#) $p < 0.05$ compared with MA. **B.** Apoptosis assay with FITC Annexin V and PI in T84 and MCF-7 cells. Cells untreated were established as negative control. Results are shown as mean ± S.D. of triplicate cultures. (*) $p < 0.05$ compared with negative control and (#) $p < 0.05$ compared with MA.

of polymer. Fig. 6A includes SEM images of PLA and TMA-PLA NFs at different magnification. As it is observed, uniform and smooth NFs were observed in both substrates, with a total absence of beads.

The average fiber diameter as well as the fiber diameter distribution was determined for PLA and TMA-PLA NFs (see Figure S5). The incorporation of the chemotherapeutic drug produced a increase in the average fiber diameter, from 468 to 538 nm (an increase of ~ 15 %). SEM images for PCL and TMA-PCL NFs are included in Fig. 6A. As observed, smooth and uniform NFs were observed for both substrates. The average fiber diameter and the fiber diameter distribution was also determined (see Figure S6). Again, a small increase in the fiber diameter was obtained after the TMA incorporation, resulting in 487.5 nm for PCL and 595.5 nm TMA-PCL (an increase of ~ 22 %). It is important to note that the increase comparing pure PLA and PCL was only ~ 4 %, and the increase for TMA-PLA and TMA-PCL was ~ 10 %. The increase between PLA and PCL suggests that the higher amount of polymer used for PCL produce an increase in fiber diameter.

An important disadvantage of PLA is its high hydrophobicity, which limits the application in biological media. With the aim to reduce the hydrophobicity, it is normally mixed with hydrophilic polymers during the electrospinning process. The most used polymers are chitosan [81], polyethylene glycol (PEG) [82], polyethylene oxide (PEO) [83–85], or poly(vinyl alcohol) (PVA) [86], or poly (vinyl pyrrolidone) PVP [43,87,88], among others. In this work, and with the aim to reduce the PLA hydrophobicity, it has been mixture with poly(vinyl pyridine) PVP. Table 1 includes the amount of PLA and PVP used during the electrospinning process for the fabrication of the PLA/PVP and TMA-PLA/PVP NFs. Fig. 6 shows SEM images at different magnification for PLA/PVP and for TMA-PLA/PVP NFs. Homogeneous and well-distributed NFs were observed for both polymeric samples. The average fiber diameter and the fiber diameter distribution was also determined (see Figure S7). As in the previous cases, a small increase in the fiber diameter was obtained after the drug incorporation, resulting in 829 nm for PLA/PVP NFs and 972.1 nm for TMA-PLA/PVP NFs. Interestingly, the fiber diameter for the PLA/PVP mixture was higher compared with that for PLA and PCL NFs, probably due to the presence of the PVP in the polymeric mixture.

Concerning the interaction between PLA and PVP it is important to mention that previously investigated structures focused on the fabrication of PLA nanofibers in the presence of hydrophilic polymers have determine a core/sheath structure. In specific, Kyuchyuk et al. prepared nanofibrous composites from PEO, PLA, and beeswax (BW) by single electrospinning of their homogeneous blend solution. The produced fibers had core/double-sheath structure with a PEO core, PLA inner sheath and BW outer sheath [85]. Bonan et al. investigated the antimicrobial activity of electrospun nanofibers composed by poly(lactic acid)/polyvinylpyrrolidone nanofibers loaded with Copaiba [88]. They fabricated nanofibers with different PVP concentrations, and they found interesting results of fiber diameter analyses indicating that the addition of PVP led to an increase in average fiber diameter as compared to pure PLA fibers. This suggests a similar core/sheath structure where the PLA in located in the center and the PVP in the external part of the nanofiber, thus increasing the fiber diameter with the amount of PVP. Oliveira et al. studied the properties of nanofibers produced by mixtures of PLA and PEO fabricated by blend electrospinning.[84] The fiber diameters were smallest in the neat polymers, and TEM investigations revealed a core/sheath structure form sample mixture. These results suggest that in our specific case we probably have a polymeric nanofiber with core/sheath structure where the interaction is produced with the PLA is located in the center and the PVP in the external part of the nanofiber.

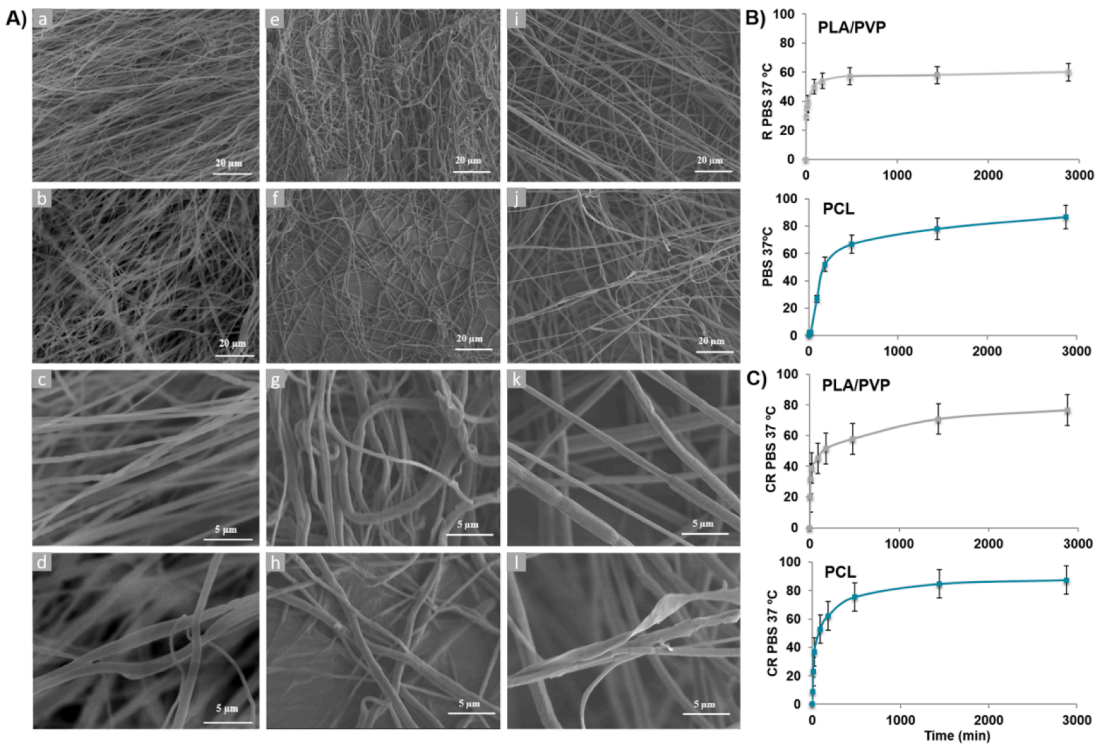

Fig. 6. SEM images of NFs (**A**). "a" and "c", PLA NFs; "b" and "d", TMA-PLA NFs, "e" and "g"; PCL NFs; "f" and "h", TMA-PCL NFs, "I" and "k"; PLA/PVP NFs; "j" and "l", TMA-PLA/PVP NFs. In vitro release in PBS of TMA included in PCL and PLA/PVP NFs: continuous (**B**) and cumulative (**C**) release. Data were represented as the mean value ± SD of triplicate measurements.

3.7. Drug encapsulation efficiency

To determine the TMA encapsulation efficiency in different NFs, HPLC technique was used. For each NF, measurements in triplicate were performed and the concentration of TMA in each sample was estimated using a previously made calibration curve. The amount of TMA (in mg) per mg of each NF was: 0.029 mg TMA/mg PLA, 0.027 mg TMA/mg PCL and 0.024 mg TMA/mg PLA/PVP.

3.8. Drug release assay

Results for continuous and cumulative release measurements of TMA at 37 °C in PBS media are shown in Fig. 6. In continuous release process, TMA release percentage from PLA/PVP fibbers quickly reaches values around 40 %, in only 20 min, having a maximum release of 60 %, which is reached after 500 min (8 h, Fig. 6B, PLA/PVP). In case of PCL fibbers, release is slightly slower, only reaching 40 % after 2 h of treatment, having a maximum of 87 % after 48 h (Fig. 6B, PCL). These results can be explained by a stronger interaction of TMA with PLC during the first minutes of release, probably due to the easier hydrogen bond formation among hydroxyl groups in TMA with the less hindered oxygen atoms in PCL, if compared to these in PLA/PVP. However, after longer period of time, hydrogen bonds are replaced by water, remaining only π-π interactions between phenyl groups of tyramine and vinylpryridine. This interaction avoids a complete release of TMA from PLA/PVP fibbers, with a maximum of 60 % (Fig. 6B, PLA/PVP).

As expected, cumulative release of TMA is fast from both fibbers (Fig. 6C), as corresponds to more favoured repartition constants. It is worth to mention that cumulative release from PCL reaches about 40 % in only 20 min, when this percentage was only reached after 2 h in continuous release. This fact can be explained by faster hydrogen bond compensation when water media is replaced, and consequently an easier release of TMA. Again, after long periods of PBS treatment at 37 °C, maximum release of TMA from PLA/PVP is slower (77 % at 48 h, Fig. 6C, PLA-PVP) than that for PCL (87 % at 48 h, Fig. 6C, PCL), as correspond to the remaining π-π interactions.

3.9. Degradation analysis

TMA-PLA/PVP and TMA-PCL exhibited 30.4 % and 20.7 % loss weight respectively after 9 days of incubation (Table 4). Our results suggest that the developed nanofibers are degradable as they reduced their mass with respect to the beginning of the experiment as has been observed in similar nanoformulations [89,90].

3.10. In vitro TMA-loaded NFs cytotoxic activity

The cytotoxicity of the NFs synthetized by electrospinning was tested in mouse fibroblasts cells L929 and in human tumor cell lines T84 and MCF-7 during 48 h of treatment. As shown in Fig. 7, in all cell lines NFs without drug had no significant toxicity ($p < 0.05$). This means that in all cell lines tested NFs were biocompatible. Importantly, both TMA-loaded NFs had an antiproliferative effect in all cell lines. TMA-loaded PLA/PVP NFs significantly reduced cell proliferation in T84, MCF-7, and L929 cells (47.93 %, 44.84 % and 47.35 % respectively), and TMA-loaded PCL NFs also reduced cells proliferation with 36.73 %, 25.12 % and 38.25 % in T84, MCF-7 and L929 cells respectively ($p < 0.001$). The cell anti-proliferation effect values are higher in the TMA-loaded PLA/PVP NFs compared with the PCL nanofibers. It is expected that the polymeric NFs may increase the localized availability of drug in the medium in an progressive way, so that they can be used for longer treatment times

Table 4
Analysis of NFs weight loss after 9 days of incubation in culture medium.

NF sample	Total weight (mg)	Dried weight (mg)	NF loss weight (mg)
TMA-PLA/PVP	24.00	16.70	7.30
TMA-PCL	24.00	19.03	4.97

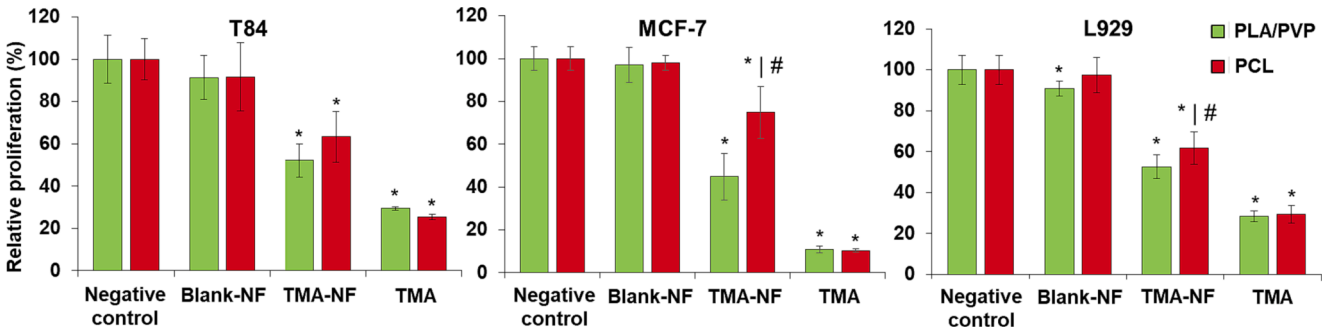

Fig. 7. Relative proliferation of cells treated with blank PLA/PVP and blank PCL NFs, free TMA, TMA-PLA/PVP NFs and TMA-PCL NFs for 48 h. Data were represented as the mean values ± SD of six cultures. (*) $p < 0.05$ compared with control cells, (#) $p < 0.05$ compared with blank PLA/PVP NF.

[91,92]. Chi et al. synthesized PLA NFs loaded with paclitaxel to study its potential antiproliferative effect against colorectal carcinoma cells HCT-116 during 24 h, achieving a decrease of the tumor cell population by up to 36 % compared to untreated cells [93]. Interestingly, Sedghi et al. loaded curcumin in PVA and chitosan NFs which resulted in up to 100 % cell inhibition after 96 h of treatment against MCF-7 BC, L929 fibroblasts and HEP G2 hepatoblastoma cells [91,93] which reveals its potential as an antitumor treatment. The development of this type of NFs could be used for local implementation after tumor resection. Ye et al. synthesized NFs based on PLGA and loaded with DOX which were tested in *in vivo* models of Balb/c nude mice, in which subcutaneous tumors were generated from HT29 CRC cell line and surgically removed when the tumor diameter was approximately 1 cm. After resection, 5 mg of NF was applied at the tumor site and, after 14 and 19 days, PLGA-NF was found to be biocompatible and DOX-loaded NFs reduced and prevented tumor recurrence [94].

4. Conclusion

In this work, we have fabricated an implantable polymeric dressing material for potential applications in LDD. A TMA derivative has been incorporated into polymeric PLA/PVP and PCL NFs by the electrospinning technique, obtaining biocompatible and biodegradable polymeric mats with antitumor activity against BC and CRC cells. In specific it has been found an important antiproliferation effect in T84, MCF-7 and L929 cancer cell lines, being also biocompatible with non-tumour cells. Better antiproliferation results were obtained for the mixture PLA/PVP compared with the fibres containing PCL, probably due to the high hydrophilicity of PVP. In addition, TMA has been found to be much less genotoxic than its predecessor MA, which could suggest a possible difference in the mechanisms of action through which TMA and MA carry out their cytotoxic effect. Therefore, TMA-loaded NFs could be of great interest against different types of solid tumors such as BC or CRC. However, further studies would be needed to clarify numerous unknowns.

Declaration of Competing Interest

The authors declare that they have no known competing financial interests or personal relationships that could have appeared to influence the work reported in this paper.

Data availability

No data was used for the research described in the article.

Acknowledgments

This work was supported in part by the Junta de Andalucía, FEDER program [A-CTS-666-UGR20, P20_00540, B-CTS-122-UGR20]; the Spanish Ministry of Science, Innovation and Universities [RTC2019-006870-1]; the Instituto de Salud Carlos III [PI19/01478-FEDER, PMPTA22/00136]. C.L. acknowledges the ISCIII for the P-FIS [ref. PI20-00284]. A.C acknowledges the Ministerio de Educación, Ciencia y Deporte y Competitividad (Spain) for the FPU2019 grant [FPU19/04112]. L.L.C., M.M., V.G.R. and M.F. would like to thank Comunidad de Madrid for the predoctoral grant IND2020/BIO-17523. M.F. is grateful to Instituto de Salud Carlos III (ISCIII) for project No DTS20/00109 (AES20-ISCIII) and PI22/00789 (AES22-ISCIII). Funding for open access charge: University of Granada / CBUA.

Appendix A. Supplementary material

Supplementary data to this article can be found online at https://doi.org/10.1016/j.ejpb.2023.11.011.

References

[1] X. Bai, Y. Zhang, H. Jiang, P. Yang, H. Li, Y. Zhang, P. He, Effects of maslinic acid on the proliferation and apoptosis of A549 lung cancer cells, Mol. Med. Rep. 13 (2016) 117–122, https://doi.org/10.3892/mmr.2015.4552.
[2] Y. Tian, H. Xu, A.A. Farooq, B. Nie, X. Chen, S. Su, R. Yuan, G. Qiao, C. Li, X. Li, X. Liu, X. Lin, Maslinic acid induces autophagy by down-regulating HSPA8 in pancreatic cancer cells, Phytother. Res. 32 (2018) 1320–1331, https://doi.org/10.1002/ptr.6064.
[3] R. Jain, A. Grover, Maslinic acid differentially exploits the MAPK pathway in estrogen-positive and triple-negative breast cancer to induce mitochondrion-mediated, caspase-independent apoptosis, Apoptosis 25 (2020) 817–834, https://doi.org/10.1007/s10495-020-01636-y.
[4] F.J. Reyes-Zurita, G. Pachón-Peña, D. Lizárraga, E.E. Rufino-Palomares, M. Cascante, J.A. Lupiáñez, The natural triterpene maslinic acid induces apoptosis in HT29 colon cancer cells by a JNK-p53-dependent mechanism, BMC Cancer 11 (2011) 154, https://doi.org/10.1186/1471-2407-11-154.
[5] E.E. Rufino-Palomares, F.J. Reyes-Zurita, L. García-Salguero, K. Mokhtari, P. P. Medina, J.A. Lupiáñez, J. Peragón, Maslinic acid, a triterpenic anti-tumoural agent, interferes with cytoskeleton protein expression in HT29 human colon-cancer cells, J. Proteomics 83 (2013) 15–25, https://doi.org/10.1016/j.jprot.2013.02.031.
[6] I. Serbian, B. Siewert, A. Al-Harrasi, R. Csuk, 2-O-(2-chlorobenzoyl) maslinic acid triggers apoptosis in A2780 human ovarian carcinoma cells, Eur. J. Med. Chem. 180 (2019) 457–464, https://doi.org/10.1016/j.ejmech.2019.07.049.
[7] S. Sommerwerk, L. Heller, C. Kerzig, A.E. Kramell, R. Csuk, Rhodamine B conjugates of triterpenoic acids are cytotoxic mitocans even at nanomolar concentrations, Eur. J. Med. Chem. 127 (2017) 1–9, https://doi.org/10.1016/j.ejmech.2016.12.040.
[8] D. Fuentes-Rios, A. Cepero, M. García-Castro, R. Contreras-Cáceres, J.M. López-Romero, C. Luque, L. Cabeza, C. Melguizo, J. Prados, Synthesis, solubility and antitumor activity of maslinic acid derivatives, Eur. J. Med. Chem. Rep. 4 (2022), 100032, https://doi.org/10.1016/j.ejmcr.2022.100032.
[9] H. Sung, J. Ferlay, R.L. Siegel, M. Laversanne, I. Soerjomataram, A. Jemal, F. Bray, Global cancer statistics 2020: GLOBOCAN estimates of incidence and mortality worldwide for 36 cancers in 185 countries, CA Cancer J. Clin. (2021), https://doi.org/10.3322/caac.21660.
[10] K.D. Miller, L. Nogueira, A.B. Mariotto, J.H. Rowland, K.R. Yabroff, C.M. Alfano, A. Jemal, J.L. Kramer, R.L. Siegel, Cancer treatment and survivorship statistics, 2019, CA Cancer J. Clin. 69 (2019) 363–385, https://doi.org/10.3322/caac.21565.
[11] J. Zugazagoitia, C. Guedes, S. Ponce, I. Ferrer, S. Molina-Pinelo, L. Paz-Ares, Current challenges in cancer treatment, Clin. Ther. 38 (2016) 1551–1566, https://doi.org/10.1016/j.clinthera.2016.03.026.

[12] L. Fuccio, D. Rex, T. Ponchon, L. Frazzoni, M. Dinis-Ribeiro, P. Bhandari, E. Dekker, M. Pellisè, L. Correale, J. van Hooft, R. Jover, D. Libanio, F. Radaelli, S. Alfieri, F. Bazzoli, C. Senore, J. Regula, T. Seufferlein, T. Rösch, P. Sharma, A. Repici, C. Hassan, New and recurrent colorectal cancers after resection: a systematic review and meta-analysis of endoscopic surveillance studies, Gastroenterology 156 (2019) 1309–1323.e3, https://doi.org/10.1053/j.gastro.2018.12.006.
[13] R. Contreras-Cáceres, L. Cabeza, G. Perazzoli, A. Díaz, J.M. López-Romero, C. Melguizo, J. Prados, Electrospun nanofibers: recent applications in drug delivery and cancer therapy, Nanomaterials 9 (2019) 656, https://doi.org/10.3390/nano9040656.
[14] J.B. Wolinsky, Y.L. Colson, M.W. Grinstaff, Local drug delivery strategies for cancer treatment: gels, nanoparticles, polymeric films, rods, and wafers, J. Control. Release 159 (2012) 14–26, https://doi.org/10.1016/j.jconrel.2011.11.031.
[15] S. Raju, M. Manalel Joseph, R.P. Kuttanpillai, H. Padinjarathil, P. Gopalakrishnan Nair Usha, S. Therakathinal Thankappan Nair, Polysaccharide enabled biogenic fabrication of pH sensing fluorescent gold nanoclusters as a biocompatible tumor imaging probe, Microchim Acta. 187 (2020) 246. https://doi.org/10.1007/s00604-020-4189-8.
[16] F.-M. Chen, M. Zhang, Z.-F. Wu, Toward delivery of multiple growth factors in tissue engineering, Biomaterials 31 (2010) 6279–6308, https://doi.org/10.1016/j.biomaterials.2010.04.053.
[17] S.-H. Lee, H. Shin, Matrices and scaffolds for delivery of bioactive molecules in bone and cartilage tissue engineering, Adv. Drug Deliv. Rev. 59 (2007) 339–359, https://doi.org/10.1016/j.addr.2007.03.016.
[18] G. Gainza, S. Villullas, J.L. Pedraz, R.M. Hernandez, M. Igartua, Advances in drug delivery systems (DDSs) to release growth factors for wound healing and skin regeneration, Nanomedicine 11 (2015) 1551–1573, https://doi.org/10.1016/j.nano.2015.03.002.
[19] R.Y. Tam, T. Fuehrmann, N. Mitrousis, M.S. Shoichet, Regenerative therapies for central nervous system diseases: a biomaterials approach, Neuropsychopharmacol. 39 (2014) 169–188, https://doi.org/10.1038/npp.2013.237.
[20] R. Bouhajeb, A.C. Abreu, S. Selmi, C. Gerke, A. Bellalah, A. Alvear-Jiménez, L. Lozano Chamizo, M. Marciello, G. Villaverde, A.I. Tristán, L. Chekir-Ghedira, I. Fernández, R. Contreras-Caceres, Implantable electrospun nanofibers with wound-healing capabilities in the reduction of pressure ulcers, ACS Appl. Polym. Mater. 5 (2023) 429–440, https://doi.org/10.1021/acsapm.2c01585.
[21] Y. Ning, W. Shen, F. Ao, Application of blocking and immobilization of electrospun fiber in the biomedical field, RSC Adv. 10 (2020) 37246–37265, https://doi.org/10.1039/D0RA06865A.
[22] P.G. Shikhi-Abadi, M. Irani, A review on the applications of electrospun chitosan nanofibers for the cancer treatment, Int. J. Biol. Macromol. 183 (2021) 790–810, https://doi.org/10.1016/j.ijbiomac.2021.05.009.
[23] C. Hu, S. Liu, Y. Zhang, B. Li, H. Yang, C. Fan, W. Cui, Long-term drug release from electrospun fibers for in vivo inflammation prevention in the prevention of peritendinous adhesions, Acta Biomater. 9 (2013) 7381–7388, https://doi.org/10.1016/j.actbio.2013.03.040.
[24] M.V. Jose, V. Thomas, K.T. Johnson, D.R. Dean, E. Nyairo, Aligned PLGA/HA nanofibrous nanocomposite scaffolds for bone tissue engineering, Acta Biomater. 5 (2009) 305–315, https://doi.org/10.1016/j.actbio.2008.07.019.
[25] E.-Y.-S. See, S.L. Toh, J.C.H. Goh, Simulated intervertebral disc-like assembly using bone marrow-derived mesenchymal stem cell sheets and silk scaffolds for annulus fibrosus regeneration, J. Tissue Eng. Regen. Med. 6 (2012) 528–535, https://doi.org/10.1002/term.457.
[26] B.D. Ulery, L.S. Nair, C.T. Laurencin, Biomedical applications of biodegradable polymers, J Polym Sci B 49 (2011) 832–864, https://doi.org/10.1002/polb.22259.
[27] F. Zheng, S. Wang, S. Wen, M. Shen, M. Zhu, X. Shi, Characterization and antibacterial activity of amoxicillin-loaded electrospun nano-hydroxyapatite/poly (lactic-co-glycolic acid) composite nanofibers, Biomaterials 34 (2013) 1402–1412, https://doi.org/10.1016/j.biomaterials.2012.10.071.
[28] T.J. Sill, H.A. von Recum, Electrospinning: Applications in drug delivery and tissue engineering, Biomaterials 29 (2008) 1989–2006, https://doi.org/10.1016/j.biomaterials.2008.01.011.
[29] N. Bhardwaj, S.C. Kundu, Electrospinning: a fascinating fiber fabrication technique, Biotechnol. Adv. 28 (2010) 325–347, https://doi.org/10.1016/j.biotechadv.2010.01.004.
[30] H.H. Huang, C.L. He, H.S. Wang, X.M. Mo, Preparation of core-shell biodegradable microfibers for long-term drug delivery, J. Biomed. Mater. Res. - Part a. 90 (2009) 1243–1251, https://doi.org/10.1002/jbm.a.32543.
[31] J. Xie, C.H. Wang, Electrospun micro- and nanofibers for sustained delivery of paclitaxel to treat C6 glioma in vitro, Pharm. Res. 23 (2006) 1817–1826, https://doi.org/10.1007/s11095-006-9036-z.
[32] Y. Chen, J. Hu, F. Zeng, J. Wei, Y. Chen, Novel controlled drug delivery system for multiple drugs based on electrospun nanofibers containing nanomicelles, J. Biomater. Sci. Polym. Ed. 25 (2014) 257–268, https://doi.org/10.1080/09205063.2013.852367.
[33] W. Li, T. Luo, Y. Yang, X. Tan, L. Liu, Formation of controllable hydrophilic/hydrophobic drug delivery systems by electrospinning of vesicles, Langmuir 31 (2015) 5141–5146, https://doi.org/10.1021/la504796v.
[34] K. Qiu, C. He, W. Feng, W. Wang, X. Zhou, Z. Yin, L. Chen, H. Wang, X. Mo, Doxorubicin-loaded electrospun poly(l-lactic acid)/mesoporous silica nanoparticles composite nanofibers for potential postsurgical cancer treatment, J. Mater. Chem. B 1 (2013) 4601–4611, https://doi.org/10.1039/c3tb20636j.
[35] C.L. Zhang, F.H. Cao, J.L. Wang, Z.L. Yu, J. Ge, Y. Lu, Z.H. Wang, S.H. Yu, Highly stimuli-responsive Au nanorods/poly(N-isopropylacrylamide) (PNIPAM) composite hydrogel for smart switch, ACS Appl. Mater. Interfaces 9 (2017) 24857–24863, https://doi.org/10.1021/acsami.7b05223.
[36] A. Gerber, M. Bundschuh, D. Klingelhofer, D.A. Groneberg, Gold nanoparticles: recent aspects for human toxicology, J. Occupat. Med. Toxicol. 8 (2013) 1–6, https://doi.org/10.1186/1745-6673-8-32.
[37] G.U. Preethi, B.S. Unnikrishnan, J. Sreekutty, M.G. Archana, M.S. Anupama, R. Shiji, K. Raveendran Pillai, M.M. Joseph, H.P. Syama, T.T. Sreelekha, Semi-interpenetrating nanosilver doped polysaccharide hydrogel scaffolds for cutaneous wound healing, Int. J. Biol. Macromol. 142 (2020) 712–723, https://doi.org/10.1016/j.ijbiomac.2019.10.012.
[38] Z.Q. Feng, C. Shi, B. Zhao, T. Wang, Magnetic electrospun short nanofibers wrapped graphene oxide as a promising biomaterials for guiding cellular behavior, Mater. Sci. Eng. C 81 (2017) 314–320, https://doi.org/10.1016/j.msec.2017.08.015.
[39] A. Hervault, N.T.K. Thanh, Magnetic nanoparticle-based therapeutic agents for thermo-chemotherapy treatment of cancer, Nanoscale 6 (2014) 11553–11573, https://doi.org/10.1039/c4nr03482a.
[40] Y. Yu, L. Kong, L. Li, N. Li, P. Yan, Antitumor activity of doxorubicin-loaded carbon nanotubes incorporated poly(lactic-co-glycolic acid) electrospun composite nanofibers, Nanoscale Res. Lett. 10 (2015), https://doi.org/10.1186/s11671-015-1044-7.
[41] T. Zhang, M. Tang, S. Zhang, Y. Hu, H. Li, T. Zhang, Y. Xue, Y. Pu, Systemic and immunotoxicity of pristine and PEGylated multi-walled carbon nanotubes in an intravenous 28 days repeated dose toxicity study, Int. J. Nanomed. 12 (2017) 1539–1554, https://doi.org/10.2147/IJN.S123345.
[42] M. Radmansouri, E. Bahmani, E. Sarikhani, K. Rahmani, F. Sharifianjazi, M. Irani, Doxorubicin hydrochloride - Loaded electrospun chitosan/cobalt ferrite/titanium oxide nanofibers for hyperthermic tumor cell treatment and controlled drug release, Int. J. Biol. Macromol. 116 (2018) 378–384, https://doi.org/10.1016/j.ijbiomac.2018.04.161.
[43] B. Nim, P. Sreearunothai, Preparation of TiO 2 -loaded electrospun fibers of polylactide / poly (vinylpyrrolidone) blends for use as catalysts in epoxidation of unsaturated oils, (2018).
[44] A.M. Gañán-Calvo, J. Dávila, A. Barrero, Current and droplet size in the electrospraying of liquids. Scaling laws, J. Aerosol Sci 28 (1997) 249–275, https://doi.org/10.1016/S0021-8502(96)00433-8.
[45] R. Vasita, D.S. Katti, Nanofibers and their applications in tissue engineering, Int. J. Nanomed. 1 (2006) 15–30, https://doi.org/10.2147/nano.2006.1.1.15.
[46] P. Berndt, G.B. Fields, M. Tirrell, Synthetic lipidation of peptides and amino acids: monolayer structure and properties, J. Am. Chem. Soc. 117 (1995) 9515–9522, https://doi.org/10.1021/ja00142a019.
[47] R. Zhang, P.X. Ma, Synthetic nano-fibrillar extracellular matrices with predesigned macroporous architectures, J. Biomed. Mater. Res. 52 (2000) 430–438, https://doi.org/10.1002/1097-4636(200011)52:2<430::AID-JBM25>3.0.CO;2-L.
[48] J. Huang, Syntheses and applications of conducting polymer polyaniline nanofibers, Pure Appl. Chem. 78 (2006) 15–27, https://doi.org/10.1351/pac200678010015.
[49] S. Elmehrath, H.L. Nguyen, S.M. Karam, A. Amin, BioMOF-based anti-cancer drug delivery systems, Nanomaterials 13 (2023) 953.
[50] F. Safdari, P.J. Carreau, M.C. Heuzey, M.R. Kamal, Effects of poly(ethylene glycol) on the morphology and properties of biocomposites based on polylactide and cellulose nanofibers, Cellul. 24 (2017) 2877–2893, https://doi.org/10.1007/s10570-017-1327-5.
[51] Z. Guo, Z. Wang, Y. Qin, J. Zhang, Y. Qi, B. Liu, W. Pan, Fabrication of biodegradable nanofibers via melt extrusion of immiscible blends, E-Polymers 22 (2022) 733–741, https://doi.org/10.1515/epoly-2022-0059.
[52] A. Elamparithi, A.M. Punnoose, S. Kuruvilla, M. Ravi, S. Rao, S.F.D. Paul, Electrospun polycaprolactone matrices with tensile properties suitable for soft tissue engineering, Artif. Cells Nanomed. Biotechnol. 44 (2016) 878–884, https://doi.org/10.3109/21691401.2014.998825.
[53] H. Wang, Y. Feng, Z. Fang, W. Yuan, M. Khan, Co-electrospun blends of PU and PEG as potential biocompatible scaffolds for small-diameter vascular tissue engineering, Mater. Sci. Eng. C 32 (2012) 2306–2315, https://doi.org/10.1016/j.msec.2012.07.001.
[54] F. Zheng, S. Wang, M. Shen, M. Zhu, X. Shi, Antitumor efficacy of doxorubicin-loaded electrospun nano-hydroxyapatite–poly(lactic-co-glycolic acid) composite nanofibers, Polym. Chem. 4 (2013) 933–941, https://doi.org/10.1039/C2PY20779F.
[55] S. Homaeigohar, M. Monavari, B. Koenen, A.R. Boccaccini, Biomimetic biohybrid nanofibers containing bovine serum albumin as a bioactive moiety for wound dressing, Mater. Sci. Eng. C Mater. Biol. Appl. 123 (2021), 111965, https://doi.org/10.1016/j.msec.2021.111965.
[56] M.J. Mochane, T.S. Motsoeneng, E.R. Sadiku, T.C. Mokhena, J.S. Sefadi, Morphology and properties of electrospun PCL and its composites for medical applications: a mini review, Appl. Sci. 9 (2019) 2205, https://doi.org/10.3390/app9112205.
[57] N.P. Singh, M.T. McCoy, R.R. Tice, E.L. Schneider, A simple technique for quantitation of low levels of DNA damage in individual cells, Exp. Cell Res. 175 (1988) 184–191, https://doi.org/10.1016/0014-4827(88)90265-0.
[58] J.T. Wilson, P.L. Pascoe, J.M. Parry, D.R. Dixon, Evaluation of the comet assay as a method for the detection of DNA damage in the cells of a marine invertebrate, Mytilus edulis L. (Mollusca: Pelecypoda), Mutation Research/Fundamental and Molecular Mechanisms of Mutagenesis 399 (1998) 87–95, https://doi.org/10.1016/S0027-5107(97)00268-6.
[59] P. Skehan, R. Storeng, D. Scudiero, A. Monks, J. McMahon, D. Vistica, J.T. Warren, H. Bokesch, S. Kenney, M.R. Boyd, New colorimetric cytotoxicity assay for

anticancer-drug screening, J. Natl Can. Inst. 82 (1990) 1107–1112, https://doi.org/10.1093/jnci/82.13.1107.
[60] S. Sommerwerk, L. Heller, J. Kuhfs, R. Csuk, Urea derivates of ursolic, oleanolic and maslinic acid induce apoptosis and are selective cytotoxic for several human tumor cell lines, Eur. J. Med. Chem. 119 (2016) 1–16, https://doi.org/10.1016/j.ejmech.2016.04.051.
[61] M. Kozubek, I. Serbian, S. Hoenke, O. Kraft, R. Csuk, Synthesis and cytotoxic evaluation of hydroxycinnamic acid rhodamine B conjugates, Resul. Chem. 2 (2020), 100057, https://doi.org/10.1016/j.rechem.2020.100057.
[62] I.Z. Pavel, R. Csuk, C. Danciu, S. Avram, F. Baderca, A. Cioca, E.-A. Moacă, C.-V. Mihali, I. Pinzaru, D.M. Muntean, C.A. Dehelean, Assessment of the antiangiogenic and anti-inflammatory properties of a maslinic acid derivative and its potentiation using zinc chloride, Int. J. Mol. Sci. 20 (2019) 2828, https://doi.org/10.3390/ijms20112828.
[63] F.J. Reyes-Zurita, E.E. Rufino-Palomares, L. García-Salguero, J. Peragón, P. P. Medina, A. Parra, M. Cascante, J.A. Lupiáñez, Maslinic acid, a natural triterpene, induces a death receptor-mediated apoptotic mechanism in Caco-2 p53-deficient colon adenocarcinoma cells, PLoS One 11 (2016) e0146178.
[64] B. del Rio, B. Redruello, V. Ladero, S. Cal, A.J. Obaya, M.A. Alvarez, An altered gene expression profile in tyramine-exposed intestinal cell cultures supports the genotoxicity of this biogenic amine at dietary concentrations, Sci. Rep. 8 (2018) 17038, https://doi.org/10.1038/s41598-018-35125-9.
[65] M. Ortega-Muñoz, F. Rodríguez-Serrano, E. De los Reyes-Berbel, N. Mut-Salud, F. Hernández-Mateo, A. Rodríguez-López, J.M. Garrido, F.J. López-Jaramillo, F. Santoyo-González, Biological Evaluation and Docking Studies of Synthetic Oleanane-type Triterpenoids, ACS Omega. 3 (2018) 11455–11468. https://doi.org/10.1021/acsomega.8b01034.
[66] B. Siewert, E. Pianowski, A. Obernauer, R. Csuk, Towards cytotoxic and selective derivatives of maslinic acid, Bioorg. Med. Chem. 22 (2014) 594–615, https://doi.org/10.1016/j.bmc.2013.10.047.
[67] Y. Lu, Y. Liu, C. Yang, Evaluating in vitro DNA damage using comet assay, J. Vis. Exp. (2017) 56450, https://doi.org/10.3791/56450.
[68] U. Plappert-Helbig, S. Libertini, W. Frieauff, D. Theil, H.-J. Martus, Gamma-H2AX immunofluorescence for the detection of tissue-specific genotoxicity in vivo, Environ. Mol. Mutagen. 60 (2019) 4–16, https://doi.org/10.1002/em.22238.
[69] A. Sharma, K. Singh, A. Almasan, Histone H2AX phosphorylation: a marker for DNA damage, Methods Mol. Biol. 920 (2012) 613–626, https://doi.org/10.1007/978-1-61779-998-3_40.
[70] K.-W. Lu, M.-D. Yang, S.-F. Peng, J.-C. Chen, P.-Y. Chen, H.-Y. Chen, T.-J. Lu, F.-S. Chueh, J.-C. Lien, K.-C. Lai, K.-C. Liu, Y.-Y. Tai, Maslinic acid induces DNA damage and impairs DNA repair in human cervical cancer HeLa cells, Antican. Res 40 (2020) 6869–6877. https://doi.org/10.21873/anticanres.14709.
[71] D.B. Wang, C. Kinoshita, Y. Kinoshita, R.S. Morrison, p53 and mitochondrial function in neurons, Biochimica et Biophysica Acta (BBA) - Molecular Basis of Disease (2014) 1186–1197, https://doi.org/10.1016/j.bbadis.2013.12.015.
[72] R. Roskoski, Vascular endothelial growth factor (VEGF) and VEGF receptor inhibitors in the treatment of renal cell carcinomas, Pharmacol. Res. 120 (2017) 116–132, https://doi.org/10.1016/j.phrs.2017.03.010.
[73] C. Li, Z. Yang, C. Zhai, W. Qiu, D. Li, Z. Yi, L. Wang, J. Tang, M. Qian, J. Luo, M. Liu, Maslinic acid potentiates the anti-tumor activity of tumor necrosis factor α by inhibiting NF-κB signaling pathway, Mol. Cancer 9 (2010) 73, https://doi.org/10.1186/1476-4598-9-73.
[74] C.-C. Lin, C.-Y. Huang, M.-C. Mong, C.-Y. Chan, M.-C. Yin, Antiangiogenic potential of three triterpenic acids in human liver cancer cells, J. Agric. Food Chem. 59 (2011) 755–762, https://doi.org/10.1021/jf103904b.
[75] P. Thakor, W. Song, R.B. Subramanian, V.R. Thakkar, D.A. Vesey, G.C. Gobe, Maslinic acid inhibits proliferation of renal cell carcinoma cell lines and suppresses angiogenesis of endothelial cells, J. Kidney Can. VHL. 4 (2017) 16–24. https://doi.org/10.15586/jkcvhl.2017.64.
[76] K.K. David, S.A. Andrabi, T.M. Dawson, V.L. Dawson, Parthanatos, a messenger of death, Front Biosci. (landmark Ed). 14 (2009) 1116–1128, https://doi.org/10.2741/3297.
[77] K. Newton, K.E. Wickliffe, D.L. Dugger, A. Maltzman, M. Roose-Girma, M. Dohse, L. Kőműves, J.D. Webster, V.M. Dixit, Cleavage of RIPK1 by caspase-8 is crucial for limiting apoptosis and necroptosis, Nature 574 (2019) 428–431, https://doi.org/10.1038/s41586-019-1548-x.
[78] B. Tummers, D.R. Green, Caspase-8: regulating life and death, Immunol. Rev. 277 (2017) 76–89, https://doi.org/10.1111/imr.12541.
[79] M. Medina-O'Donnell, F. Rivas, F.J. Reyes-Zurita, A. Martinez, J.A. Lupiañez, A. Parra, Diamine and PEGylated-diamine conjugates of triterpenic acids as potential anticancer agents, Eur. J. Med. Chem. 148 (2018) 325–336. https://doi.org/10.1016/j.ejmech.2018.02.044.
[80] T. Uto, A. Sakamoto, N.H. Tung, T. Fujiki, K. Kishihara, S. Oiso, H. Kariyazono, O. Morinaga, Y. Shoyama, Anti-proliferative activities and apoptosis induction by triterpenes derived from eriobotrya japonica in human leukemia cell lines, Int. J. Mol. Sci. 14 (2013) 4106–4120, https://doi.org/10.3390/ijms14024106.
[81] A. Hardiansyah, H. Tanadi, M.C. Yang, T.Y. Liu, Electrospinning and antibacterial activity of chitosan-blended poly(lactic acid) nanofibers, J. Polym. Res. 22 (2015) 1–10, https://doi.org/10.1007/s10965-015-0704-8.
[82] L. Moradkhannejhad, M. Abdouss, N. Nikfarjam, M.H. Shahriari, V. Heidary, The effect of molecular weight and content of PEG on in vitro drug release of electrospun curcumin loaded PLA/PEG nanofibers, J. Drug Delivery Sci. Technol. 56 (2020), 101554, https://doi.org/10.1016/j.jddst.2020.101554.
[83] V. Allizond, G. Banche, M. Salvoni, M. Malandrino, C. Cecone, A.M. Cuffini, P. Bracco, Facile one-step electrospinning process to prepare AgNPs-loaded PLA and PLA/PEO mats with antibacterial activity, Polymers 15 (2023) 1470, https://doi.org/10.3390/polym15061470.
[84] M. Marconcini, L.H.C. Mattoso, J.E. Oliveira, E.A. Moraes, G.M. Glenn, E.S. Medeiros, Properties of Poly (lactic acid) and Poly (ethylene oxide) Solvent Polymer Mixtures and Nanofibers Made by Solution Blow Spinning, (2013) 3672–3681. https://doi.org/10.1002/app.39061.
[85] S. Kyuchyuk, D. Paneva, N. Manolova, I. Rashkov, D. Karashanova, Core / double-sheath composite fibers from, Polymers 14 (2022) 5036, https://doi.org/10.3390/polym14225036.
[86] R. Fatahian, M. Mirjalili, R. Khajavi, M.K. Rahimi, N. Nasirizadeh, Effect of electrospinning parameters on production of polyvinyl alcohol/polylactic acid nanofiber using a mutual solvent, Polym. Polym. Compos. 29 (2021) S844–S856, https://doi.org/10.1177/09673911211027126.
[87] U.D. Batista, D.E.C. Perez, R.F. Bonan, P.R.F. Bonan, Poly (lactic acid)/ poly (vinyl pyrrolidone) membranes produced by solution blow spinning : Structure , thermal , spectroscopic , and microbial barrier properties, 44802 (2017) 1–9. https://doi.org/10.1002/app.44802.
[88] R.F. Bonan, P.R.F. Bonan, A.U.D. Batista, F.C. Sampaio, A.J.R. Albuquerque, M.C. B. Moraes, L.H.C. Mattoso, G.M. Glenn, E.S. Medeiros, J.E. Oliveira, In vitro antimicrobial activity of solution blow spun poly(lactic acid)/polyvinylpyrrolidone nanofibers loaded with Copaiba (Copaifera sp.) oil, Mater. Sci. Eng. C 48 (2015) 372–377, https://doi.org/10.1016/j.msec.2014.12.021.
[89] H.J. Haroosh, Y. Dong, K.-T. Lau, Tetracycline hydrochloride (TCH)-loaded drug carrier based on PLA:PCL nanofibre mats: experimental characterisation and release kinetics modelling, J. Mater. Sci. 49 (2014) 6270–6281, https://doi.org/10.1007/s10853-014-8352-7.
[90] H.J. Haroosh, Y. Dong, S. Jasim, S. Ramakrishna, Morphological structures and drug release effect of multiple electrospun nanofibre membrane systems based on PLA PCL, and PCL/magnetic nanoparticle composites, J. Nanomater. 2022 (2022) e5190163.
[91] R. Sedghi, A. Shaabani, Z. Mohammadi, F.Y. Samadi, E. Isaei, Biocompatible electrospinning chitosan nanofibers: a novel delivery system with superior local cancer therapy, Carbohydr. Polym. 159 (2017) 1–10, https://doi.org/10.1016/j.carbpol.2016.12.011.
[92] J. Shi, P.W. Kantoff, R. Wooster, O.C. Farokhzad, Cancer nanomedicine: progress, challenges and opportunities, Nat. Rev. Cancer 17 (2017) 20–37, https://doi.org/10.1038/nrc.2016.108.
[93] H.Y. Chi, V. Chan, C. Li, J.H. Hsieh, P.H. Lin, Y.-H. Tsai, Y. Chen, Fabrication of polylactic acid/paclitaxel nano fibers by electrospinning for cancer therapeutics, BMC Chem. 14 (2020) 63, https://doi.org/10.1186/s13065-020-00711-4.
[94] C. Ye, J. Zhao, Y. Zheng, C. Wu, Y. Chen, H. Wu, X. An, M. Huang, S. Wang, Preparation of poly(lactic-co-glycolic acid)-based composite microfibers for postoperative treatment of tumor in NIR I and NIR II biowindows, Macromol. Biosci. 18 (2018) 1800206, https://doi.org/10.1002/mabi.201800206.